AD 273 798

D1-82-0122

BOEING SCIENTIFIC RESEARCH LABORATORIES

BOEING LOBE SWEEP INTERFEROMETER SYSTEM

JOHN LANSINGER

RALPH GAGNON

DECEMBER, 1961

Document 1-82-0122

B O E I N G L O B E S W E E P
I N T E R F E R O M E T E R S Y S T E M

John Lansinger
Ralph Gagnon

December, 1961

Geo-Astrophysics Laboratory

Boeing Scientific Research Laboratories

ABSTRACT

A lobe sweep interferometer system is described which has been developed at the Boeing Scientific Research Laboratories. Continuous measurements are made of the intensity of the total coherent noise received from the sun at 221 mc and the phase difference between the signals from two antennas. A phase lock method of maintaining a 1 kc difference between two mixer injection signals at 251 mc is described. A phase compensator is discussed in which a fixed phase relationship is maintained between a reference signal and the 1 kc signal resulting from a fictitious source at the predicted position of the sun. It is shown that the use of the compensator simplifies angle measurements of burst positions and facilitates measurement of the position of the radio center of the sun. Although several aspects of the system are not unique, most of the system is discussed for the sake of continuity and completeness. A discussion is given regarding the interpretation of the received data to provide position measurements of bursts in relation to solar co-ordinates. The effects of fringe blurring and correction for an extended source distribution are discussed. Several factors affecting the precision of position measurements are presented.

PREFACE

A lobe sweep interferometer system has been developed at the Boeing Scientific Research Laboratory to be used primarily for the study of electromagnetic emissions originating from the sun at meter wavelengths. The purpose of this report is to communicate to the reader the design philosophy used in the development of the Boeing system, some of the practical limitations of the system, and how the recorded data are interpreted. It is intended that this report will form the framework for reports to follow which will deal specifically with the reception and interpretations of solar data.

As it presently operates, the lobe sweep interferometer records continuously the intensities of solar radio bursts at 221 mc and their positions relative to the radio center of gravity of the sun. The measurements to date, which have been made principally to establish the feasibility of the system, have indicated the desirability of further refinements. These refinements, which are scheduled for early incorporation into the system, include increasing the baseline length, installing preamplifiers directly at the antenna terminals, and the design and construction of a device which modifies the operation of the output phase meter. This device, called a phase compensator, is currently undergoing system tests. Because of its uniqueness, the phase compensator is discussed in considerable detail in the report, even though it has not yet been finally incorporated into the lobe sweep system for routine solar observations.

TABLE OF CONTENTS

LIST OF ILLUSTRATIONS

LIST OF SYMBOLS IN ORDER OF OCCURRENCE

Part III

δ	Declination of radio center of the sun
HA	Hour angle of radio center of the sun
$\Delta\delta$	Solar coordinate along constant hour angle
ΔH	Δ HA cos δ_o, solar coordinate with constant declination
ω_a	Lobe sweep angular frequency
ϕ_a	Phase constant of system
Θ	Incident angle between ray path and baseline normal
d	Antenna baseline separation
γ	Inclination of baseline to polar axis
ξ	Position angle of baseline in equatorial plane
HA'	HA + ξ
δ_o	Declination of radio center of gravity from which burst positions are calculated, or declination of optical center of the sun
r, ψ	Solar polar coordinates
$\Delta\phi$	Phase difference between the signal from the pre-burst sun and the burst component. Also used to represent the phase shift resulting from change in the operating frequency
A, B	Multipliers in equation $\Delta\phi = A\Delta\delta + B\Delta H$. Used earlier to designate the two separate antennas.
$\Delta\chi$	Measured phase shift due to a burst
P_2/P_1	Measured ratio of intensities before and at the time of a burst

Part IV

HA_o	Hour angle of optical center of the sun
$\Delta\delta_o$	Change in declination of optical center over 24-hour period
δ'_o	Declination of optical center at t = 0
HAMS	Hour angle of the mean sun
ΔE	Change in equation of time over 24-hour period
δ_e	Equivalent angular declination error in compensator
η	Fractional error in the amplitude of the compensator phase sine wave

Part V

A	$\frac{2\pi d}{\lambda} \cos \theta_o$
θ'	Angle measured from source position θ_o
$\Delta\theta$	Source half-width
P( )	Brightness distribution of source, may be a function of time, position, and frequency
$\overline{S}$	Amplitude of lobe sweep modulation component

Appendix A

P_x	Amplitude of burst component

Appendix B

R	Source radius
D	Source diameter
A, B	Parameters used in calculating effective power
a, b	Angular functions

PART I

HISTORICAL SURVEY OF INTERFEROMETER SYSTEMS

Except for inherent simplicity, the total power interferometer has certain disadvantages, especially at low signal-to-noise levels. The shortcomings consist primarily of poor amplitude and angular resolution in the presence of non-coherent noise. In the measurement of the position of short-term radio noise enhancements of the sun, Little and Payne-Scott (1) employed a lobe sweep interferometer in which the lobe pattern from a two element interferometer was swept back and forth across a source at a constant rate by the use of a mechanical phase shifter inserted in one of the local oscillator lines.

An improvement in the capability of measuring the position and intensity of weak sources was made possible with the development of a new type of interferometer system by Ryle (2). Several configurations are possible in this new type of system, but all are characterized by the feature that the output recorder mean deviation is independent of the internal noise of the system. The mean deviation depends on the intensity of the source and the path difference between the two interferometer antennas. The statistical fluctuations about the mean are a function of the total noise in the system. These systems usually have two basic components, a device which places a tag on the coherent noise

signal in the form of amplitude modulation, and a synchronous detector which compares the received modulation component with a reference signal of the same frequency.

The phase switch system developed by Ryle (2) used a 180 degree phase switch inserted in one of the antenna legs. The phase switch varied at a step rate and produced a switch frequency modulation component in the system. The modulation component was synchronously detected at the switch frequency producing an output which was a measure of the source intensity and the position relative to the interferometer lobe pattern. An extension of the phase switch system to measure phase and therefore position continuously was made by Penfield (3) who used a servo phase control to maintain a null at the output of the synchronous detector.

Hanbury Brown, Palmer and Thompson (4) used the lobe sweep principle in addition to employing a synchronous detector to observe the position and intensity of weak radio stars. Crystal controlled local oscillator signals were used, which were separated by a small difference frequency. This accomplished the same end result as the use of a mechanical phase shifter and eliminated the problems associated with mechanical limitations. Cohen (5) used a somewhat similar instrumentation scheme in polarization measurements at 200 mc.

A further improvement in the lobe sweep system can be realized by using local oscillators which are phase locked to a constant difference frequency as was done with the Vanguard Minitrack

system (6, 7). This was accomplished in the Minitrack system by using reactance control in a voltage tunable L/C oscillator circuit.

Continuous phase measurements using a lobe sweep system have been made by Fleischer (8) who used a phase meter in place of a synchronous detector. This instrument is used to study the position and motion of long duration bursts at 517 mc.

A swept frequency technique discussed by Wild and Sheridan (9) has been used to measure the position and size of bursts originating from the sun over the range from 40-70 mc. The operating principle relies on the fact that the path difference between the receiving antennas is a function of the wavelength which is swept over a band at a fixed rate.

Multi-element interferometers have been used to measure directly the brightness distribution across the solar disk at meter wavelengths by Boischot (10) and Firor (11). In the multi-element interferometer system the sun moves across narrow strips which remain stationary in the sky and result from the antenna polar pattern. Since the angular separation between these strips is greater than the angular size of the sun, the system can unambiguously resolve several centers of activity emitting simultaneously, provided the secondary lobes are sufficiently attenuated. The main shortcoming of the multi-element interferometer is in the resolution of short duration bursts. Since the scan time is long compared to the duration of short term bursts, no accurate position measurements of single transient events can be carried out. For example, an intense burst occurring at a position of a secondary

lobe response will appear to an observer to be a low intensity burst at a position corresponding to the position of the main lobe. The position of noise storms can be determined indirectly by making a statistical analysis of a number of separate scans.

Two-element interferometers have been used to resolve short duration bursts by Owren (12) and Fokker (13) using total power and phase switch interferometers respectively. Both observers determined the position of active centers by noting the times and hence the position when the enhanced emission component was either in or out of phase, or at phase quadrature. Owren measured the positions relative to the position of the quiet sun which was assumed to coincide with the optical center. In later measurements Fokker measured the position relative to the optical center of the sun as distinct from the radio center of gravity.

PART II

DISCUSSION OF THE BOEING SYSTEM

General description of the system

The principle components of the Boeing system are shown in the simplified block diagram given in Figure 2.1. The lobe sweep results from the fact that the two local oscillator injection signals at approximately 251 mc are separated by 1 kc. Since phase lock is used, the difference frequency stability is determined by the 1 kc reed oscillator shown in the figure. An AGC system is employed which operates from the coherent noise signal output from a narrow band 1 kc filter. Intensity recordings are made over the range from the level of the quiet sun to power increases of 35 db above this level. This range is covered by two recorders, one for low level signals and one of extended range. A third recorded output, resembling in form a sine wave and herein called the interferometer output, is that from the synchronous detector. This output is used chiefly as an indication of proper system operation.

The fourth recorded output is from the phase meter and is an analog representation of the phase difference between the 1 kc coherent noise signal and the 1 kc reference signal from the phase-locked oscillators. The recorder trace is basically a sawtooth waveform. The phase compensator shown in the figure is currently being tested and has not yet been incorporated into the system for routine solar observations. It represents

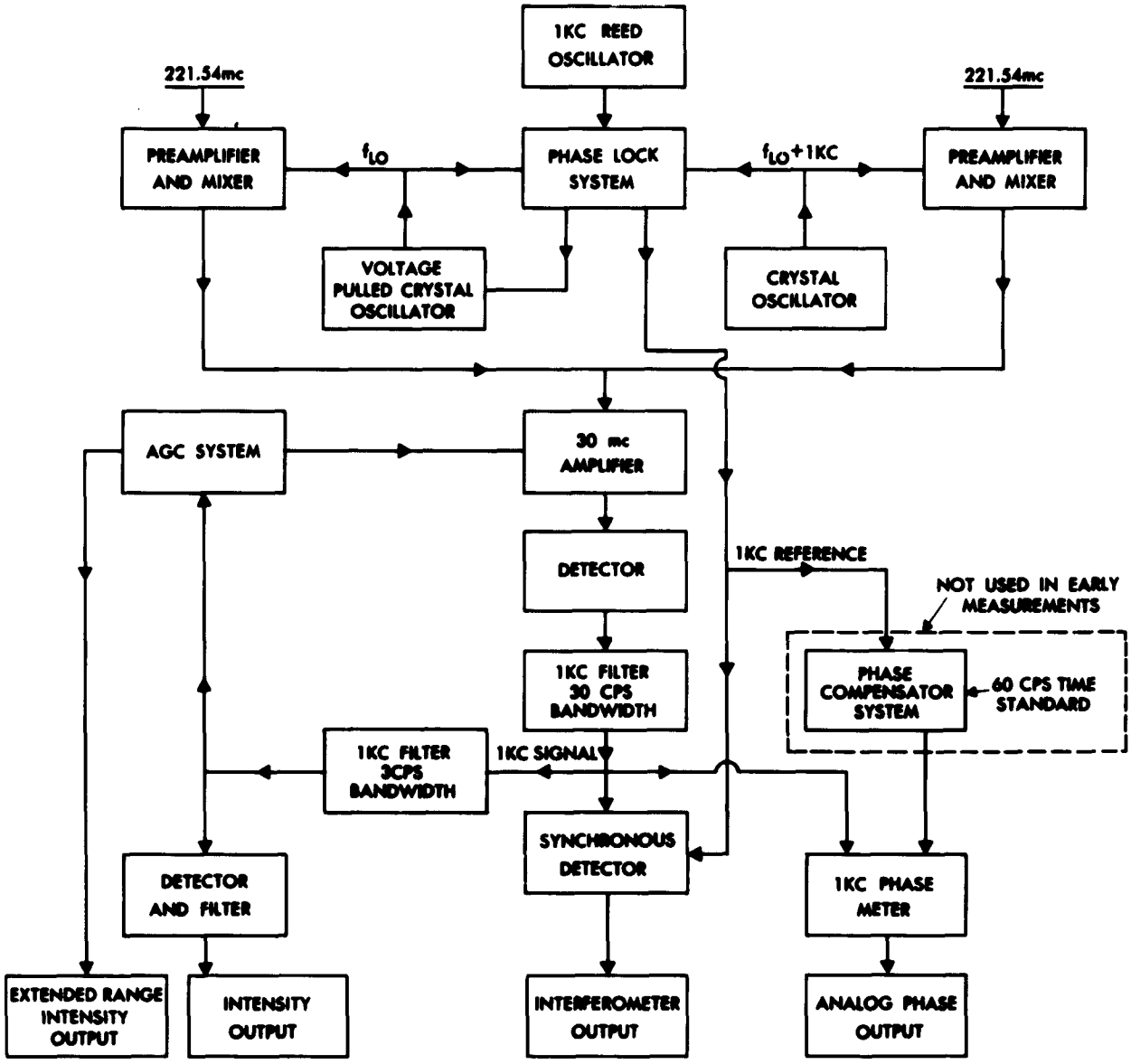

BLOCK DIAGRAM BOEING LOBE SWEEP INTERFEROMETER SYSTEM

FIG. 2.1

an improvement over the present phase meter system, in that is will remove the phase discontinuity from the present sawtooth waveform and it will enable the phasemeter to indicate the variation in position of the radio center of gravity of the sun. The phase compensator accomplishes these by inserting into the system a time varying phase which is nearly equal to that predicted for the center of the sun as it moves relative to the antenna baseline. As the phase compensator is considered to be unique, it is discussed in detail in Part IV.

In the event of a radio burst the 1 kc signal amplitude and phase will be the resultant of the superposition of the signal from the quiet sun (pre-burst level) and that of the burst. By measuring the total intensity and phase of these superposed signals the intensity and phase of the burst are calculated. A discussion later in the report will be concerned with the interpretation of the data to provide burst positions and intensities.

A summary of the operating characteristics and the parameters of the complete system is given in Table 2.1.

Site location

The receiving site is located in a thinly populated area approximately 11 air miles from the Boeing Scientific Research Laboratories in a location comparatively removed from power lines and roads. Early field tests had established that the level of radio noise interference at meter wavelengths was

TABLE 2.1

SUMMARY OF OPERATING CHARACTERISTICS

FOR THE BOEING LOBE SWEEP SYSTEM

Nominal operating frequency	221.54 mc
Lobe sweep frequency	1 kc
IF frequency	30 mc
System noise figure	4.5 - 5.0 db
Over-all receiver bandwidth	640 kc or 125 kc
Antennas	Two 10-element Yagis, equatorial mounts
Gain	Nominally 12 db above an isotropic radiator
Separation	109.0 feet = 33.2 meters
Regularly recorded outputs	
Intensity	80% full scale = 100 x 10^{-22} $wm^{-2}(cps)^{-1}$ (quasi-logarithmic)
Extended range intensity	Full scale = 31,600 x 10^{-22} $wm^{-2}(cps)^{-1}$ (quasi-logarithmic)
Analog phase	Proportional to the phase difference between the two receiving antennas
Available recording time constants	.25, .5, 1.0, 2, and 4 seconds

sufficiently low that the site would be satisfactory for solar observations.

Antennas

Two 10-element Yagi antennas are used (Taco, Y-103M) which have a gain of 10-12 db above that of an isotropic radiator. Although the nominal impedance of these antennas is 50 ohms, it was found that at 221 mc the terminal impedance was 36 ohms, necessitating pi-matching transformers to match the antennas to the 50 ohm transmission line. Each antenna is mounted to a polar axis and driven by a sidereal clock drive. RG8/U coaxial cables are used at present above ground between the antennas and the preamplifiers. The initial antenna separation is approximately 109 feet.

Pre-amplifiers

The pre-amplifiers together with the remainder of the systems are housed in a 24-foot trailer central to the antenna baseline. The pre-amplifiers are of conventional design consisting of two stages of grounded grid 7077 planar triodes, followed by a 7077 mixer and a single 6AK5 IF amplifier. Using an "L" type (14) input transformer to the pre-amplifiers, the transfer ratio was experimentally adjusted to obtain an optimum noise figure. A noise figure in the range of 4.5-5.0 db can be maintained in routine operation of the equipment.

Allowing for cable losses and an antenna gain of 10 db, the minimum detectable level (using the criteria given by Ryle and Vonberg, (15)) is approximately 10^{-23} $wm^{-2}cps^{-1}$ for a receiver

bandwidth of 600 mc, a recording time constant of 0.5 second, and a 4.8 db noise figure. Using the same antennas but placing the pre-amplifiers at the antennas would result in an improvement in the sensitivity by a factor of 2.5.

I. F. amplifier

A standard commercial 30 mc amplifier manufactured by Lel is used in the system. Over-all IF bandwidths of 125 and 640 kc are available from a crystal and a conventional L/C filter respectively.

Local oscillator system

The phase lock system is a closed-loop feedback system which is used to produce two local oscillator signals at approximately 251 mc which are separated by a fixed 1 kc difference frequency. A block diagram of the phase-lock system is given in Figure 2.2.

As shown in the figure, the two fundamental frequencies are generated in fifth overtone crystal controlled Butler oscillator circuits, multiplied in doubler circuits, and mixed to obtain the difference frequency. The 1 kc difference signal is amplified and fed to a synchronous detector which is referenced to a 1 kc signal obtained from a reed controlled oscillator. The oscillation frequency in one of the Butler oscillators is controlled over a limited range by the dc control signal formed at the output of the synchronous detector as shown in the block diagram.

A circuit schematic of the voltage controlled crystal oscillator circuit is given in Figure 2.3. As shown, non-linear capacitors are used in the plate circuit of V_2. A change in the

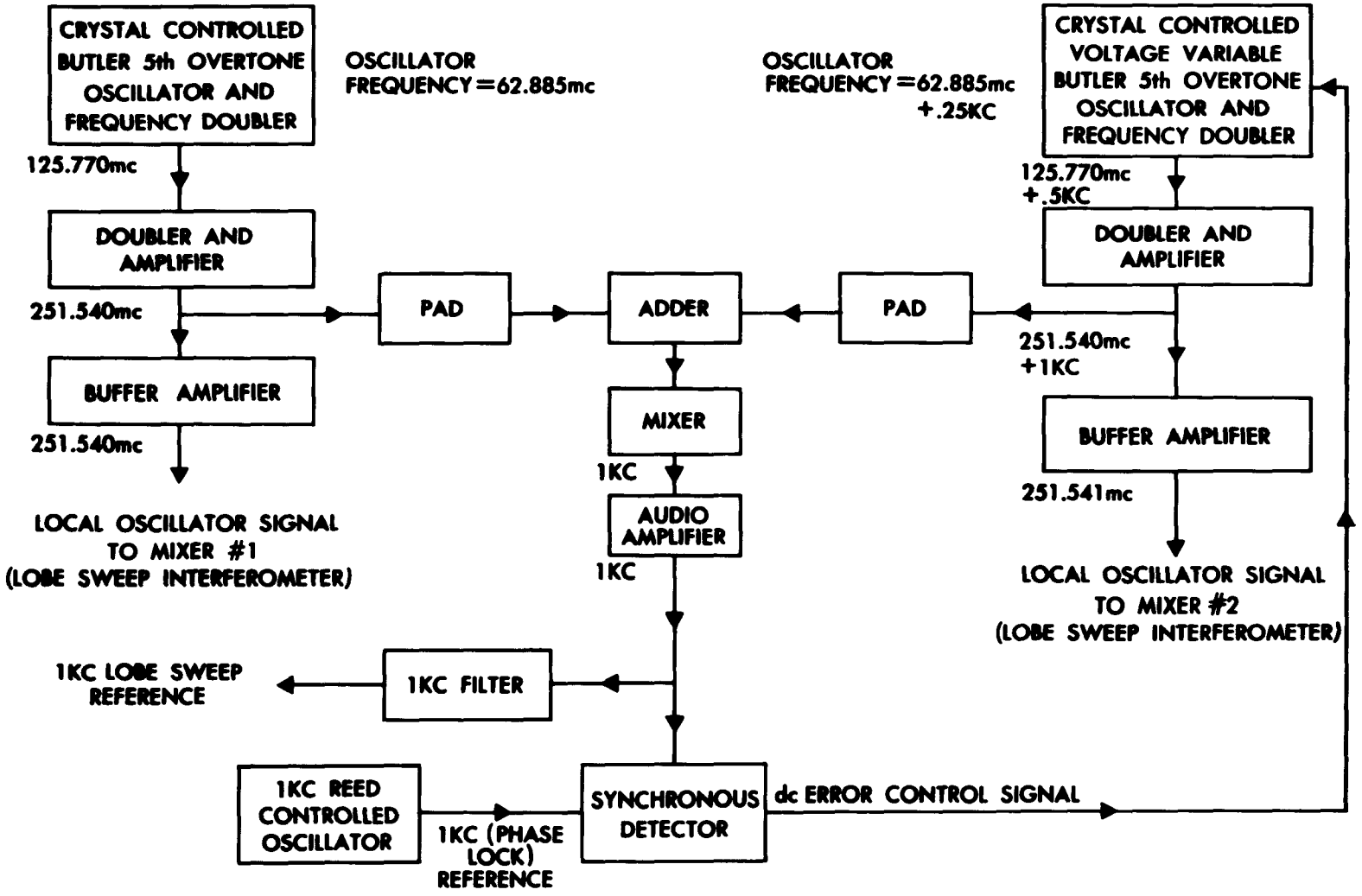

BOEING PHASE LOCK CONTROL SYSTEM

FIG. 2.2

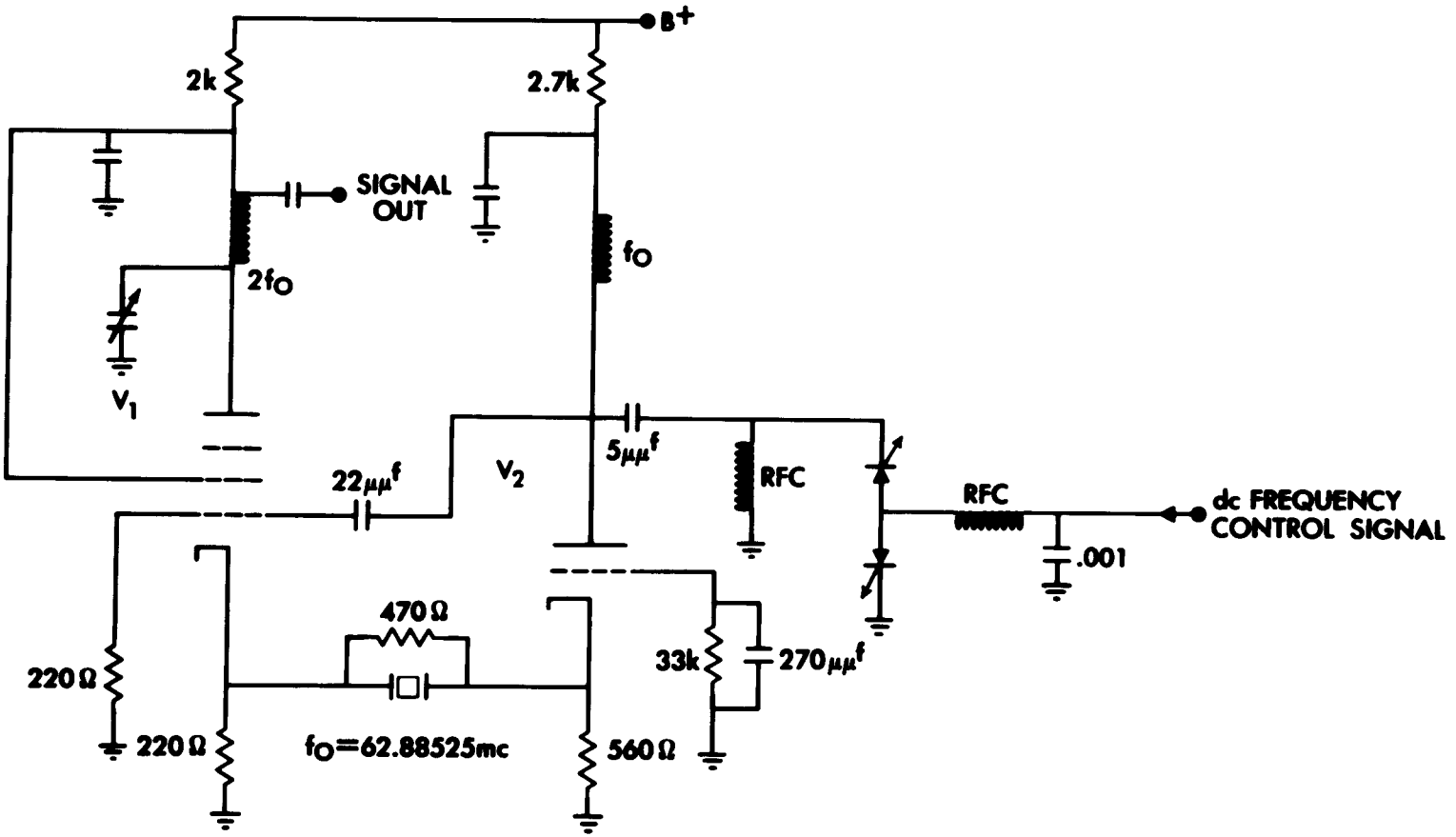

VOLTAGE PULLED CRYSTAL CONTROLLED BUTLER OSCILLATOR CIRCUIT

FIG. 2.3

dc potential applied to non-linear capacitors in the plate circuit of V_2 will produce a change in capacity and result in a phase shift in the oscillator feedback loop. The phase shift results in a small change in the oscillator frequency to achieve phase-lock equilibrium.

The polarity of the control signal applied to the capacitors is such that nearly a phase quadrature condition will be maintained (under closed-loop conditions) between the two input signals at the synchronous detector. Since the 1 kc reference signal used in the lobe sweep system is obtained from mixing the two local oscillator signals, it should be clear that a fixed phase relationship is maintained between this reference signal and that resulting from a source fixed relative to the antenna pattern.

Since it is possible to achieve phase lock at odd multiples of the 1 kc reed oscillator frequency, some initial adjustment is required at the time the system is placed in operation. It was found experimentally that the control range was sufficient to maintain phase lock without the use of temperature stabilized ovens for the crystals.

The frequency of the local oscillators is a function of the inherent stability of the Butler oscillators while the difference frequency stability is a function of the stability of the reed controlled oscillator (nominally $\pm$ 1.5 cps). The difference frequency will remain fixed independent of frequency drifts of the crystal oscillator frequencies as long as the drift is within the pull-in range of the voltage controlled oscillator.

The use of a crystal controlled oscillator as the basic frequency source takes advantage of the inherently high "Q" of the crystal, thereby minimizing problems associated with spurious oscillations, multiple oscillation modes and residual frequency modulation components. A high degree of shielding was required to provide adequate isolation between the two local oscillator channels. Cross coupling between the two channels will result in a residual 1 kc component in the system and can also result in spurious frequency modulation of the 1 kc difference frequency.

AGC system and intensity recorders

A block diagram outlining the AGC system is shown in Figure 2.4A. Referring to the figure, it is seen that the 1 kc modulated noise signal is amplified in the main IF amplifier, square law detected and passed through two filters 30 and 3 cps wide. The first filter is a conventional passive L/C filter. The second filter is approximately 3 cps wide and employs a bridged-"T" network in a feedback amplifier (16).

As shown in the figure, the 1 kc component of the signal after filtering is threshold detected, chopped at a 417 cps rate, amplified, and synchronously detected and filtered to obtain the dc gain control signal which is fed back to the main IF amplifier. The use of the chopper and synchronous detector allows for versatility and ensures high dc stability of the AGC delay level. The gains of the various amplifiers are set so that the low range recorder indicates approximately 20 percent full scale for quiet sun levels and has a uniform logarithmic gradient from this point to 80 percent full scale, a level

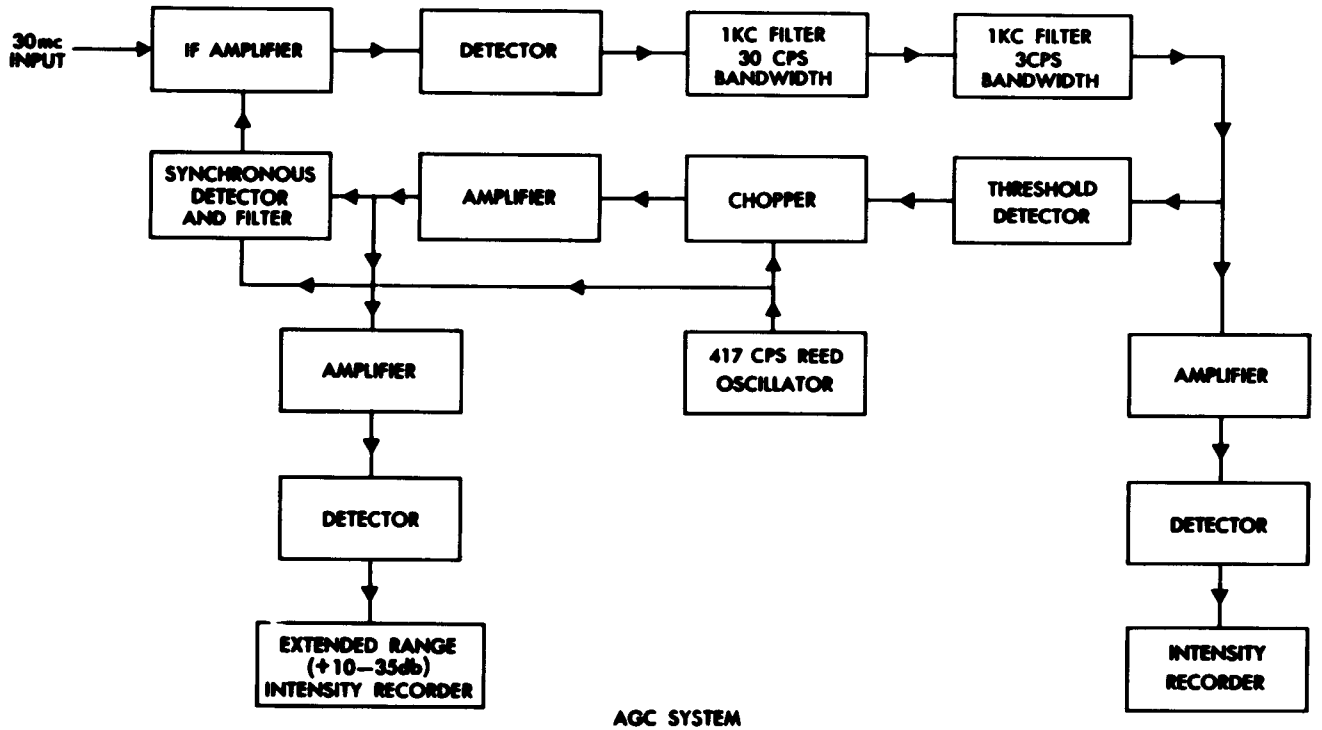

AGC SYSTEM

FIG. 2.4A

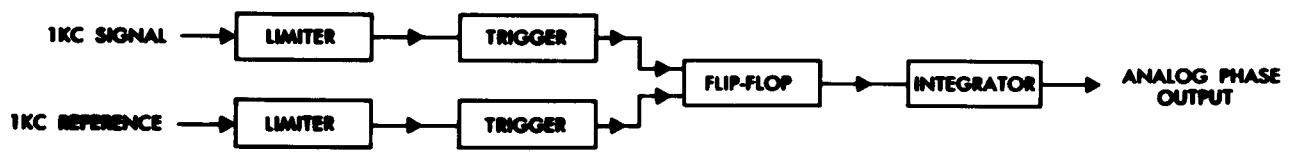

1KC PHASE METER

FIG. 2.4B

10 db above the quiet sun. The deflection of the extended range recorder shown in the block diagram is a logarithmic function of input coherent noise level above the AGC delay. Full scale deflection of this recorder corresponds to increases of approximately 35 db above that of the quiet sun.

1 kc phase meter

The 1 kc phase meter converts the phase difference between the 1 kc signal and reference to an analog voltage output. The scheme used to obtain an analog measurement of phase difference has been described before (28) and for the present circuit consists of triggering a flip-flop to turn on and off at the time of the negatively-going zero cross-over for the 1 kc reference and signal respectively. The integrated output of the flip-flop using this scheme varies linearly with phase difference, repeating itself every 2π radians. An input phase variation at a constant rate will therefore produce a sawtooth waveform at the output of the phase meter.

The flip-flop is shown in the block diagram of the phase meter in Figure 2.4B. The two trigger pulses are derived from the 1 kc reference signal and the 1 kc coherent noise signal which are amplified and limited, using cathode-coupled double-ended clipper circuits (17). The 1 kc clipped signal output from each channel is fed to bi-static transistor Schmitt triggers which fire at the zero crossing of the input signals. The square wave outputs from the Schmitt circuits are differentiated to form the triggers for the flip-flop.

Using the above scheme it is found that the output of the analog phase recording is comparatively insensitive to changes in input power level. The output deflection changes a maximum of 1 percent over an input power range of 0 - 35 db increase above that of the quiet sun.

The signal input to the phase meter, as shown in Figure 2.1, comes from a 1 kc filter, which has a bandwidth of 30 cps. The 30 cps bandwidth is sufficiently narrow to prevent multiple zero crossovers in the signal. The presence of internal noise will result in phase modulation only of the signal at the output of the limiter shown in the phase meter block diagram. The phase modulation will result in statistical fluctuations of the analog phase output, with the mean output representing the true phase difference between the reference and 1 kc signal in the absence of noise.

Calibration system

The system is calibrated to measure power levels relative to an arbitrary level output from a 5722 saturated noise diode. This calibration level is chosen to represent a level of power output close to that expected for the quiet sun. By comparing this power level with the power received from Cassiopeia, the system is calibrated to measure flux density in units of watts per square meter per cycle per second. From (18), the level received from Cassiopeia was taken to be $1.0 \times 10^{-22} wm^{-2}(cps)^{-1}$ at a frequency of 221 mc. The zero db or "quiet sun" level is ten times the level from Cassiopeia.

Two levels of power are inserted at the input to the preamplifiers each hour. These levels correspond to that of the quiet sun and the quiet sun plus 10 db. The output of a wide-band 220 mc amplifier serves to provide the +10 db calibration level. A daily check is made to determine the variations of the noise output of the amplifier relative to the noise calibration diode. Stability tests and spot daily checks have established that both the long and short term output noise stability from the amplifier are within 1 db. The amplifier has approximately 40 db gain and consists of 4 stages of grounded grid 7077's. This comparatively large available output noise power is used in checking the response and calibration of the system over a 35 db range. Calibration levels of 20, 30, and 35 db are inserted into the system once per day. Stability tests are performed on a daily basis.

All the rf switching is accomplished through the use of motor driven coaxial switches. A variable line stretcher is used to cancel out the effect of the cross coupled components, via the common noise calibration source, between the two preamplifiers. In practice, the variable line stretcher is experimentally adjusted for a null output on the intensity recording. The null is sufficiently below the quiet sun level in the system that no appreciable error is introduced in intensity measurements.

PART III

CONSIDERATIONS RELATING TO POSITION MEASUREMENTS

Introduction

This section of the report deals with the geometrical considerations relevant to the determination of burst position. The system of coordinates is so chosen that the results can be applied to an interferometer of arbitrary orientation. The derived results are also used in the analysis of the phase compensator in the next part of this report. The received data are discussed and it is shown how they are interpreted to provide burst position measurements. The error in position measurements resulting from the fact that the radio and optical center of the sun may not coincide is investigated.

Solar coordinate system

With respect to a fixed observer a point on the celestial sphere can be specified by its declination (δ) and its hour angle (HA) (Figure 3.1). By virtue of the rotation of the earth the hour angle increases continuously. The declination of celestial objects is unaffected by the earth's rotation; however, the declination of the sun changes slowly due to the revolution of the earth around that body.

It will be convenient to specify a position on the sun with respect to some reference point called the "center." The axes for the reference system will be the hour circle and the parallel of declination intersecting perpendicularly at this center. Distances along the hour circle will be indicated by $\Delta\delta$. However,

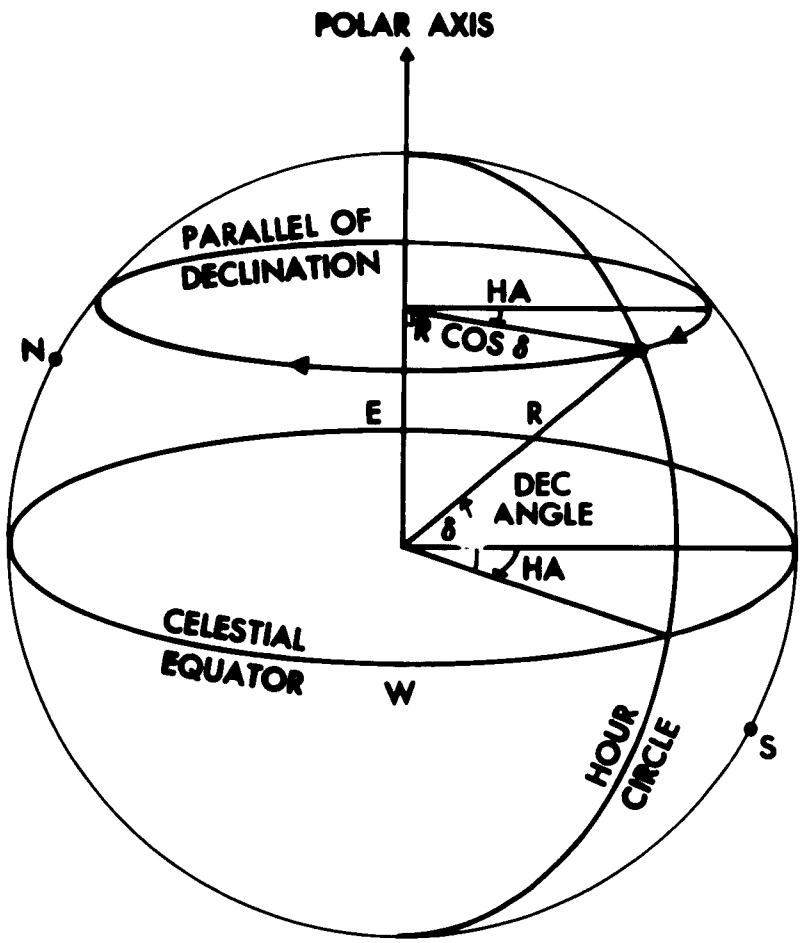

SPECIFICATION OF A POINT ON THE CELESTIAL SPHERE BY ITS DECLINATION ANGLE AND HOUR ANGLE.

FIG. 3.1

since the increment of hour angle subtended by the solar diameter increases with declination, distances along the parallel of declination will be indicated by $\Delta HA \cos \delta_o$ so that angular distances will be the same in both directions. The declination δ_o is that of the sun's center.

In general, the locus of possible source positions from interferometer data is a straight line, over angular distances of the order of the sun's diameter. This line can conveniently be specified by the length r and polar angle ψ of its normal vector from the center (Figure 3.2). ψ is measured counterclockwise from the west.

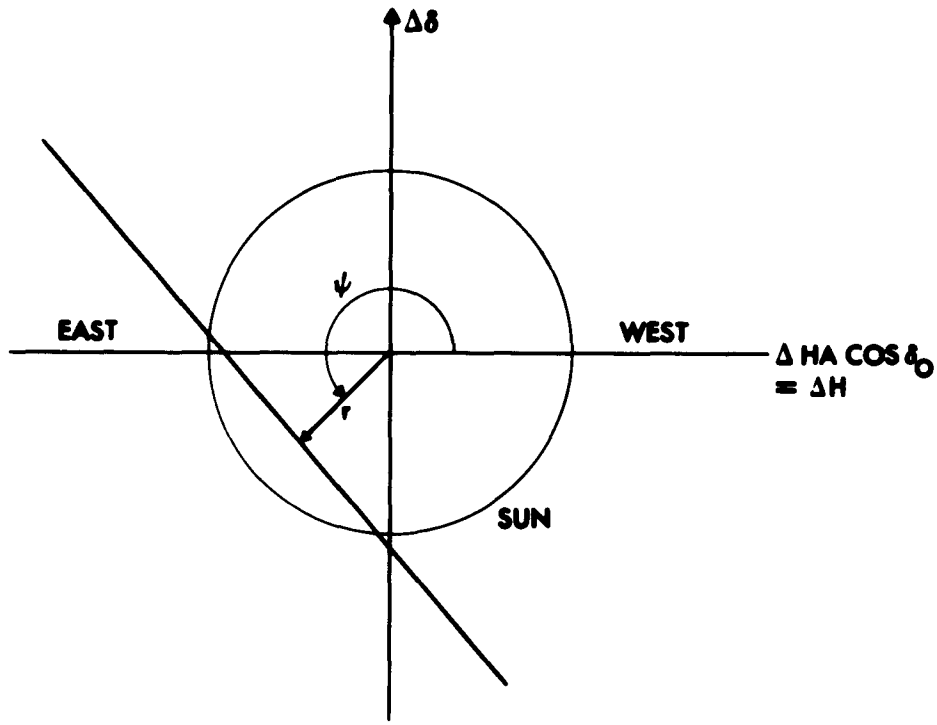

SOLAR COORDINATES

FIG. 3.2

Baseline coordinates

It is desired to calculate the position in solar coordinates of activity centers on the sun from the radio data. This calculation is dependent on the length and orientation of the interferometer baseline, which must be specified.

Given two antennas A and B, with inputs X cos $(\omega t + \phi_x)$ and Y cos $(\omega t + \phi_y)$ respectively, it can be shown that the received signal input to the phase meter is proportional to

$$XY \cos (\omega_a t - \phi_x + \phi_y + \phi_a)$$

where ϕ_a is a constant relative phase difference between channels, and ω_a is the lobe sweep frequency. The antenna A is defined as the antenna whose phase subtracts, while B is the antenna whose phase adds, so that the phase meter reads directly the quantity $(-\phi_x + \phi_y + \phi_a)$.

Define the baseline as a vector extending from A to B. Then this vector is the parameter necessary for conversion from radio data to solar coordinates.

The baseline vector will be specified by its length, its inclination γ to the polar axis, and its position angle ξ measured from the north point in the equatorial plane westward to the projection of the vector in the equatorial plane (Figure 3.3).

Derivation of the incident angle

The phase difference between the two interferometer antennas depends on the incident angle θ between the plane normal to the baseline and the incident ray. This angle will be considered positive if the ray path to the B antenna is shorter than the path to the A antenna, and negative otherwise.

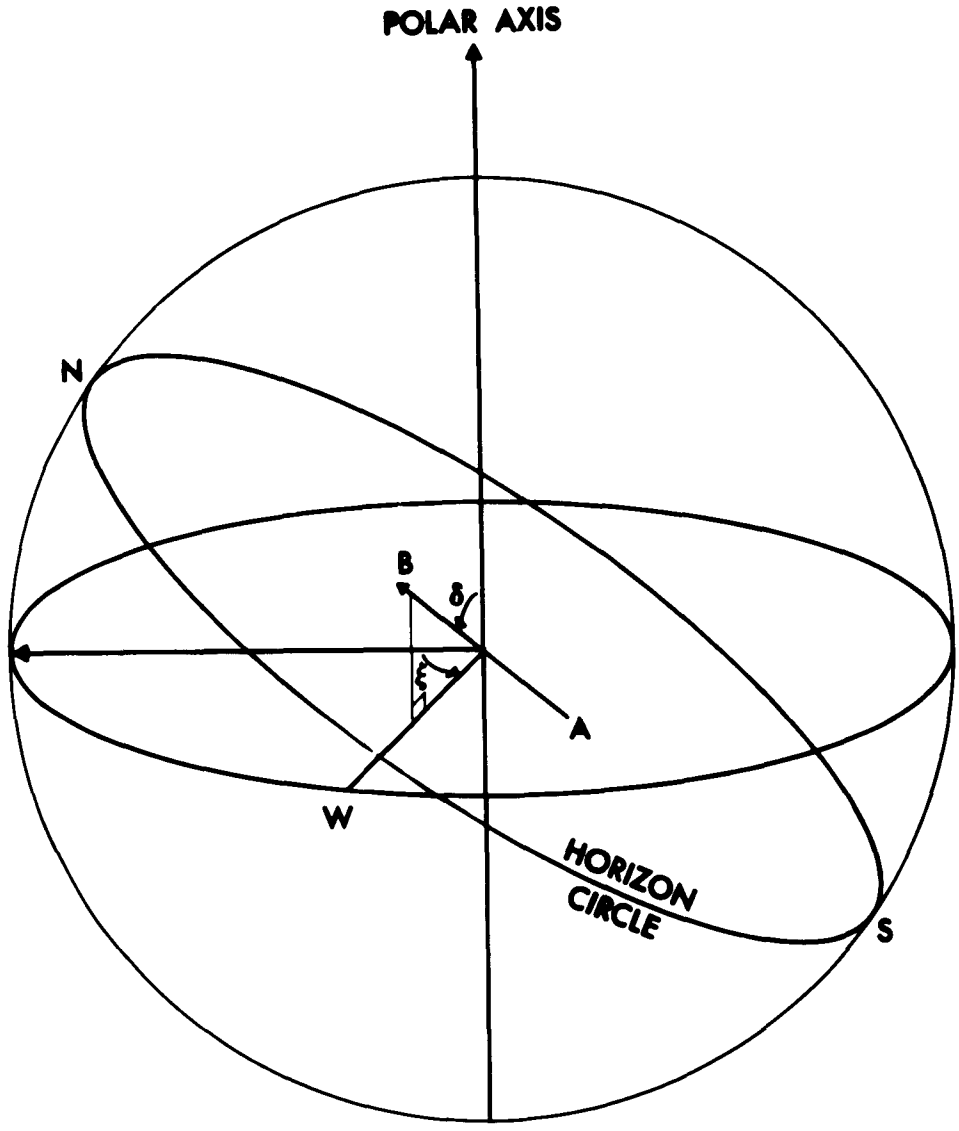

SPECIFICATION OF BASELINE ORIENTATION

FIG. 3.3

Figure 3.4 is a geometrical diagram of the relationships involved between sun position and incident angle. This is a diagram formed by looking approximately normally at both the polar axis and the baseline. From this diagram it can be seen that

3.1 $\sin \Theta = \sin \delta \cos \gamma - \cos \delta \cos (HA + \xi) \sin \gamma$

From the angle Θ, the quantity $\phi_y - \phi_x$ can be found (Appendix A). The ray path difference between the antennas is d sin Θ. This represents a phase difference of $\frac{2\pi d}{\lambda} \sin \Theta$.

Therefore, $\phi_y - \phi_x = \frac{2\pi d}{\lambda} \sin \Theta$

Substituting (3.1) gives

3.2 $\phi_y - \phi_x = \frac{2\pi d}{\lambda} [\sin \delta \cos \gamma - \cos \delta \cos (HA + \xi) \sin \gamma]$

For a horizontal east-west baseline $\gamma = \xi = \frac{\pi}{2}$. Thus from (3.2) we get

3.3 $\phi_y - \phi_x = \frac{2\pi d}{\lambda} \sin HA \cos \delta$

for an east-west baseline.

<u>Conversion to solar coordinates</u>

It is desired to convert a change in $\phi_y - \phi_x$ to the solar coordinates $\Delta\delta$ and $\Delta HA \cos \delta_o$. Partially differentiating (3.2) gives

$$\Delta(\phi_y - \phi_x) = \frac{2\pi d}{\lambda} [(\cos\delta_o \cos\gamma)\Delta\delta + (\sin\delta_o \cos(HA+\xi)\sin\gamma)\Delta\delta + (\cos\delta_o \sin(HA+\xi)\sin\gamma)\Delta HA]$$

Let $\Delta HA \cos \delta_o = \Delta H$. Then

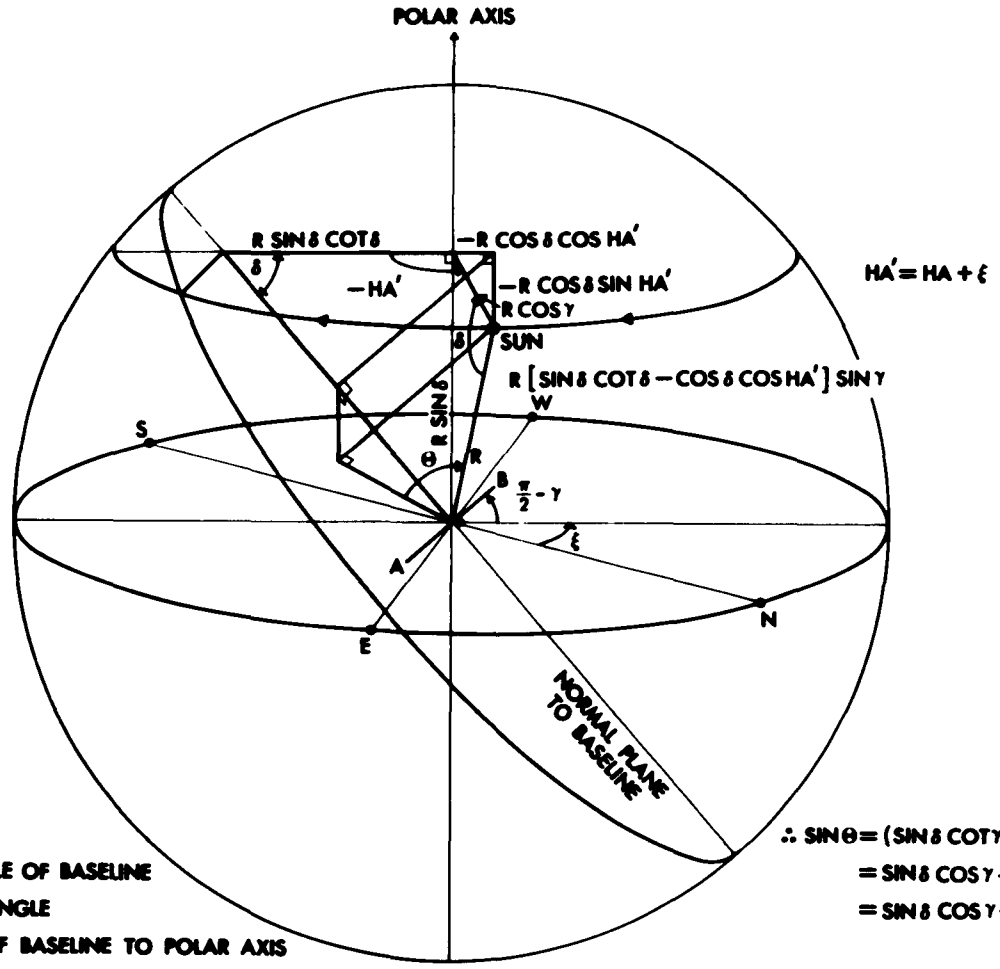

HA: HOUR ANGLE

ξ: POSITION ANGLE OF BASELINE

δ: DECLINATION ANGLE

γ: INCLINATION OF BASELINE TO POLAR AXIS

Θ: INCIDENT ANGLE OF RAY TO PLANE ⊥ TO BASELINE

$$\therefore \sin\Theta = (\sin\delta \cot\gamma - \cos\delta \cos HA') \sin\gamma$$
$$= \sin\delta \cos\gamma - \cos\delta \cos HA' \sin\gamma$$
$$= \sin\delta \cos\gamma - \cos\delta \cos(HA + \xi) \sin\gamma$$

DERIVATION OF THE INCIDENT ANGLE

FIG. 3.4

$$\Delta(\phi_y - \phi_x) = \Delta\phi = \frac{2\pi d}{\lambda}\left[(\cos\delta_o \cos\gamma + \sin\delta \cos(HA + \xi)\sin\gamma)\,\Delta\delta + \sin(HA + \xi)\sin\gamma\,\Delta H\right]$$

Thus, for a given phase meter change there is obtained the equation of a straight line specifying the location of the source. The equation is of the form

$$\Delta\phi = A\Delta\delta + B\Delta H$$

where

3.4 $$A = \frac{2\pi d}{\lambda}\left[\cos\delta_o \cos\gamma + \sin\delta_o \cos(HA + \xi)\sin\gamma\right]$$

and

3.5 $$B = \frac{2\pi d}{\lambda}\sin(HA + \xi)\sin\gamma$$

The intercepts on the ΔH and $\Delta\delta$ axes are $\frac{\Delta\phi}{B}$ and $\frac{\Delta\phi}{A}$ respectively (see Figure 3.5).

From Figure 3.5 can be found the parameters r and ψ in terms of A, B, and $\Delta\phi$:

3.6 $$\sin\psi = \frac{r}{\Delta\phi/A}$$

3.7 $$\cos\psi = \frac{r}{\Delta\phi/B}$$

Therefore

3.8 $$\psi = \tan^{-1}\frac{A}{B}$$

The angle is still ambiguous by 180° as so defined. To resolve this ambiguity, the sign of the y intercept, $\frac{\Delta\phi}{A}$, can be employed. The following rule will be used:

Rule: Assume ψ in the first or second quadrant. Compute $\frac{\Delta\phi}{A}$. If this is negative, add π to the angle.

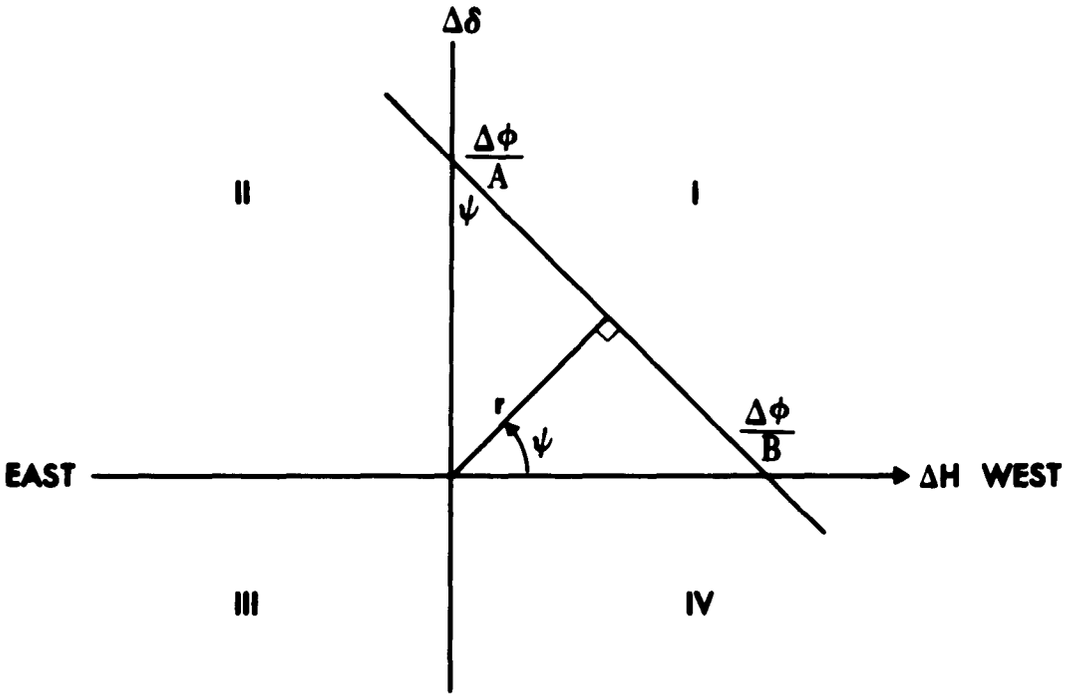

LOCUS IN SOLAR COORDINATES

FIG. 3.5

Squaring (3.6) and (3.7) and adding gives:

$$1 = \left[\frac{rB}{\Delta\phi}\right]^2 + \left[\frac{rA}{\Delta\phi}\right]^2$$

$$(\Delta\phi)^2 = r^2 (A^2 + B^2), \text{ or,}$$

$$3.9 \qquad r = \frac{\Delta\phi}{\sqrt{A^2 + B^2}}$$

Determination of burst positions from the recorded measurements

As was discussed in Section II the received data consist of two principal recordings which are:

1--An analog presentation of the phase difference of the received signal between the two receiving antennas.

2--An output which is a measure of the intensity of the total available coherent noise power.

With square-law detection the recorded phase and amplitude are the resultant of the superposition of all coherent noise sources within the primary beam of the receiving antennas. Thus the quiet sun and an enhanced component of emission will both produce a component of phase and amplitude on the two respective recordings. The phase recording will be displaced from the level due to the quiet sun if the enhanced component is not located at the position of the radio center of gravity.

A typical recording is shown in Figure 3.6. The top trace is the intensity recording. The bottom record is an analog recording of the phase measurement. The saw-tooth appearance of the phase recording results from the sun moving across the interferometer lobe pattern. Each cycle corresponds to a change

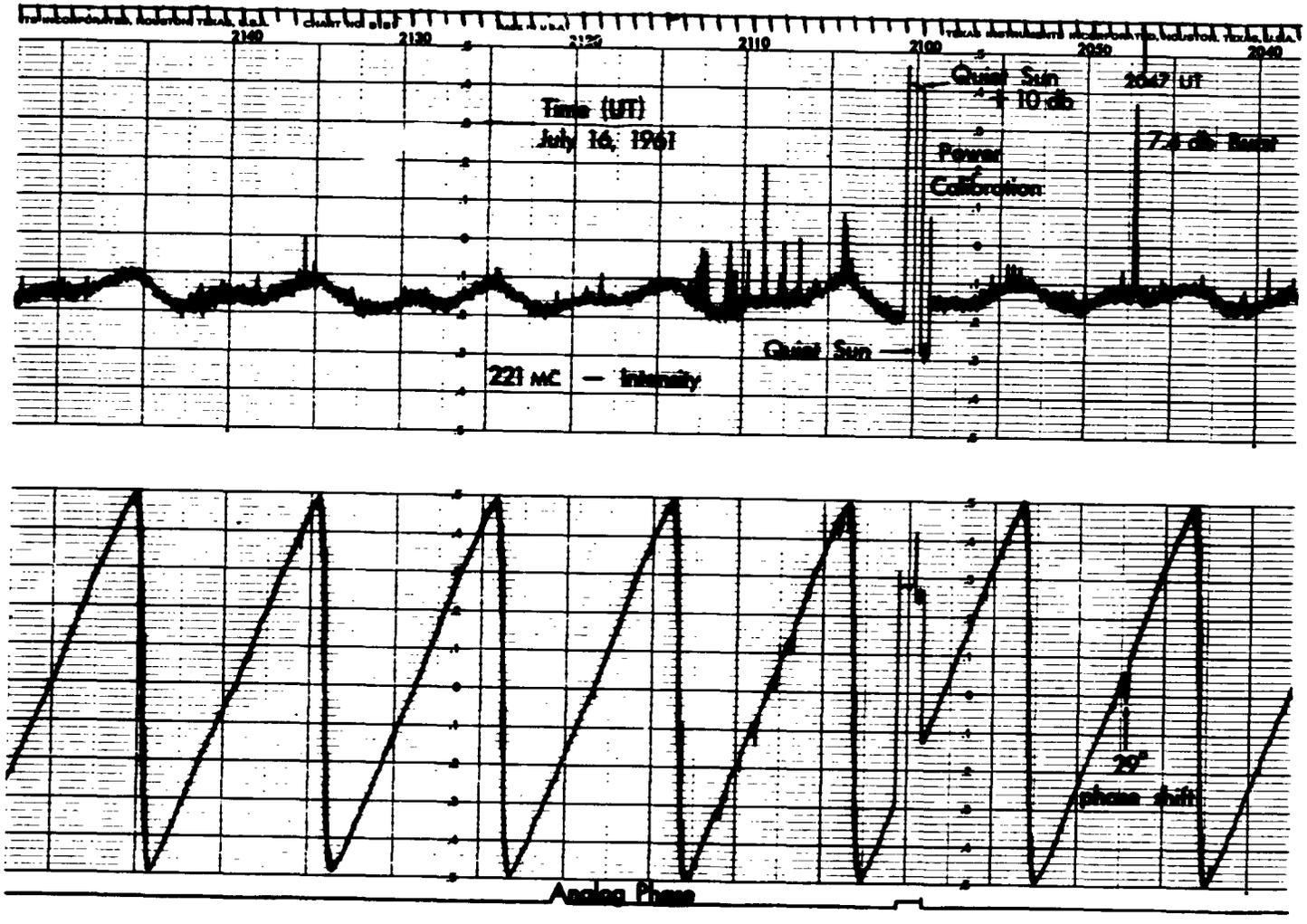

INTENSITY AND PHASE RECORDING

FIG.3.6

in path difference of the received signal between the antennas of one wave length. All of the measurements to date have been recorded in the manner shown in Figure 3.6. The phase compensator, which will be incorporated into the system shortly, will have the function of inserting into the system a variable phase nearly equal to that predicted for the optical sun. This will ideally convert the saw-tooth phase recording into a straight line.

At present the measurements of burst positions of enhanced emissions are made relative to the radio center of gravity, which, in general, does not coincide with the optical center of the sun.

The resultant amplitude and phase of the signal into the phase meter during the burst will be the superposition of two independent sine waves resulting from that of the pre-burst radio sun and that from the burst. To determine the position of the burst relative to the radio center of gravity, it is required to determine the electrical phase angle between the signal arising from the burst and that of the signal resulting from the sun in the absence of the burst. The relationship between the measured phase shift, due to the burst plus the pre-burst sun, and the phase shift of the burst component is derived in Appendix A and is

$$3.10 \qquad \Delta\phi = \tan^{-1} \frac{\frac{P_2}{P_1} \sin \Delta\chi}{\frac{P_2}{P_1} \cos \Delta\chi - 1}$$

where P_2/P_1 = measured ratio of intensities before and after burst

$\Delta\chi$ = measured phase deviation resulting from burst plus pre-burst radio sun

$\Delta\phi$ = relative phase of the burst

Referring again to Figure 3.6, showing the analog phase output, it is seen that $\Delta\chi$ is obtained simply by noting the change in phase deflection at the time of the burst. The phase shift $\Delta\chi$ is the phase shift to the new radio center of gravity, somewhere between the pre-burst center of gravity and the burst. The phase shift $\Delta\phi$, which cannot be measured, is the phase shift due to the burst alone.

Combining (3.9) and (3.10), the resultant burst position for an arbitrary baseline orientation is

$$3.11 \qquad r = \frac{\tan^{-1} \dfrac{(P_2/)_1) \sin \Delta\chi}{(P_2/P_1) \cos \Delta\chi - 1}}{(A^2 + B^2)^{1/2}}$$

For a horizontal east-west baseline $\gamma = \xi = \pi/2$ (see Figure 3.3) and from (3.4) and (3.5) we have

$$A = \frac{-2\pi d}{\lambda} \sin \delta_o \sin HA$$

$$B = \frac{2\pi d}{\lambda} \cos HA$$

Therefore from (3.9) and (3.10) for a horizontal east-west baseline, the burst position is given by

$$3.12 \qquad r = \frac{\lambda}{2\pi d} \frac{\tan^{-1} \dfrac{(P_2/P_1) \sin \Delta\chi}{(P_2/P_1) \cos \Delta\chi - 1}}{(1 - \sin^2 HA \cos^2 \delta_o)^{1/2}}$$

Similarly, the orientation angle for a horizontal east-west baseline from (3.8) is

$$3.13 \qquad \psi = \tan^{-1} (-\sin \delta_o \tan HA)$$

To illustrate the method used in the determination of burst positions, consider the 7.4 db isolated burst shown in the received data given in Figure 3.6. The relevant data relating to the burst are as follows:

declination of the sun = δ = 21° 18'

hour angle of the sun at the time of the burst = 8.25°

P_2/P_1 = 7.4 db = 5.5

measured phase shift = ΔX = 29°

operating frequency = 221.54 mc

antenna separation (horizontal east-west) = 33.2 meters = 109.0 feet

From equation (3.10) the electrical phase shift of the burst is calculated to be 34.95°. Using equation (3.12) the calculated burst position is 13.6'. From equation (3.13) the orientation angle is computed to be -2° 54'. The burst is thus located to the west of the radio center of gravity.

<u>Error in the determination of burst position resulting from an error in the assumed position of the radio center of the sun</u>

From (3.10) and (3.12), it is seen that the burst position given for a horizontal east-west baseline is

$$3.14 \qquad r = \frac{\lambda}{2\pi d} \frac{\Delta\phi}{(1 - \sin^2 HA \cos^2 \delta_o)^{1/2}}$$

and, from (3.1) this becomes

$$3.15 \qquad r = \frac{\lambda}{2\pi d} \frac{\Delta\phi}{\cos \theta}$$

The incident angle θ is the angle of the pre-burst radio center of gravity of the sun which is assumed to coincide with the solar optical center. An error in the incident angle of the radio center of gravity will result in an error in the computed burst position. From (3.15), the fractional error is

$$\frac{\Delta r}{r} = \frac{\cos \theta_o}{\cos (\theta_o + \Delta\theta)} - 1$$

From a Taylor expansion of the denominator for $\Delta\theta$ small we have

$$3.16 \qquad \frac{\Delta r}{r} \cong \frac{1}{1 - \Delta\theta \tan \theta} - 1$$

The error turns out to be negligible except for large incident angles. Given an incident angle of 85 degrees and an error in the incident angle of 15', the resulting error is 5.2 percent. Observations reported by Boischot (10) at 169 mc indicate that the maximum deviation of the center of gravity from the optical center will not exceed 1 solar radius.

PART IV

THE PHASE COMPENSATOR

Introduction

Since the phase compensator represents a major effort in the solar research program and is an innovation in interferometer instrumentation, a section of this report is devoted to the discussion of this new device. The compensator is currently undergoing tests and has not as yet been incorporated into the system for routine solar observations.

As was mentioned previously, the phase compensator will improve the performance of the system in two respects: it will remove the phase discontinuity from the present sawtooth waveform output of the phasemeter, and it will enable the phasemeter to indicate the variation in position of the radio center of gravity of the sun. The phase compensator will accomplish these by generating and inserting into the system a time-varying phase which is nearly equal to that predicted for the optical center of the sun as it moves relative to the antenna baseline. This generated time-varying phase will be subtracted from the time-varying phase of the received signal so that ideally the present sawtooth waveform of the phasemeter will be converted to a straight line.

This section of the report discusses the principle of operations of the phase compensator and the function of its various elements. The last part of this section considers the error which results from the fact that the compensator does not correct for changes

in the declination of the sun, or in the equation of time. The error is analyzed in the special case of an east-west interferometer baseline. The calibration procedure for the compensator is also discussed.

Preliminary considerations

It will be assumed for simplicity that the optical and radio centers of the sun coincide. Equation (3.2) can then be written

$$4.1 \qquad \phi_y - \phi_x = \frac{2\pi d}{\lambda}[\sin \delta_o \cos \gamma - \cos \delta_o \cos (HA_o + \xi) \sin \gamma]$$

where δ_o and HA_o are the declination and the hour angle of the optical center of the sun, respectively. The phase meter reads this value directly.

Under normal operation of the phasemeter, the largest single contribution to the recorder output is due to the second term of (4.1). This completely masks any long term variations of the sun's radio center, and in addition makes more difficult the measurement of short term variations. It is desirable, therefore, to subtract this term out. However, this must be done in such a manner that the process of subtraction does not in itself introduce appreciable error. This rules out the use of an analog device, which would permit the accumulation of error with time.

If the quantity $[-\frac{2\pi d}{\lambda} \cos \delta_o \cos (HA_o + \xi) \sin \gamma]$ is subtracted from the phase meter reading, then the phase meter will read

$$4.2 \qquad (\phi_y - \phi_x)' = \frac{2\pi d}{\lambda} \sin \delta_o \cos \gamma$$

which is almost a straight line as a function of time. Any observed deviations from a straight line would be due to changes in the position of the source alone.

The quantity $[-\frac{2\pi d}{\lambda} \cos \delta_o \sin \gamma \cos (HA_o + \xi)]$ is a quasi-sine wave, with amplitude $[-\frac{2\pi d}{\lambda} \cos \delta_o \sin \gamma]$, period of one day, and phase ξ. The term "quasi" is used because $\cos \delta_o$ varies slightly over the course of a day and HA_o does not vary linearly with time because of the equation of time perturbation.

Summary of the operating principles of the phase compensator

The phase compensator inserts into the reference signal input to the phase meter a phase shift which varies as a sine wave. This is accomplished by storing on paper tape the differences of sin HA, for 15" increments of arc, over the range of HA from 0° to 90°. Each second of time, a paper tape reader reads out this incremental difference. The difference is converted to a pulse train in which the number of pulses is proportional to the difference of sin HA read out. The resulting pulse train is fed to a ratio counter which takes out a preset fraction of the pulses sent to it. This is the method for setting the amplitude of the sine wave. The output pulses from the fractional divider are used to drive a stepping motor which in turn drives a resolver, where the subtraction mentioned earlier takes place.

The tape reader is synchronized to mean solar time with the origin of the sine wave set so that the time of maximum rate of change corresponds to meridian passage of the sun (for an east-west baseline). The operation is continuous with the tape reversing direction each 90 degrees of hour angle.

For a radio star source and a time standard synchronized to sidereal time instead of mean solar time, no day-to-day correction

would be required, as the inserted phase variation would exactly duplicate that caused by the rotation of the earth. Since the equation of time and declination of the sun change over a 24-hour period and the amplitude of the sine phase curve inserted by the compensator is constant over any one 24-hour period, it is clear that an error will develop.

The phase compensator equipment

The phase compensator consists of nine parts: (1) a paper tape input, on which is punched the sine wave data, (2) a timing system, which controls the pulse flow through the system, (3) a data counter, which converts the tape data to a pulse sequence, (4) a ratio counter, which provides a fine control of the amplitude of the sine wave by selecting a pre-determined fraction of the pulses in the sequence for removal, (5) an inhibit circuit, which inhibits the pre-determined fraction of input pulses on command from the ratio counter, (6) a divider chain, which provides coarse control of the sine-wave amplitude, (7) a stepping motor, which converts the pulse sequence to rotary motion, (8) a gear step-down box, and (9) a resolver, for converting the rotary motion to a phase subtraction. These elements will be discussed in turn. Figure 4.1 is a block diagram of the system.

Tape input

On the tape are punched values of the fifth decimal place differences between values of a sine function for consecutive 15" intervals, that is, the incremental difference punched at a given position is the difference between the value of the sine at the given position and the sum of the differences already punched.

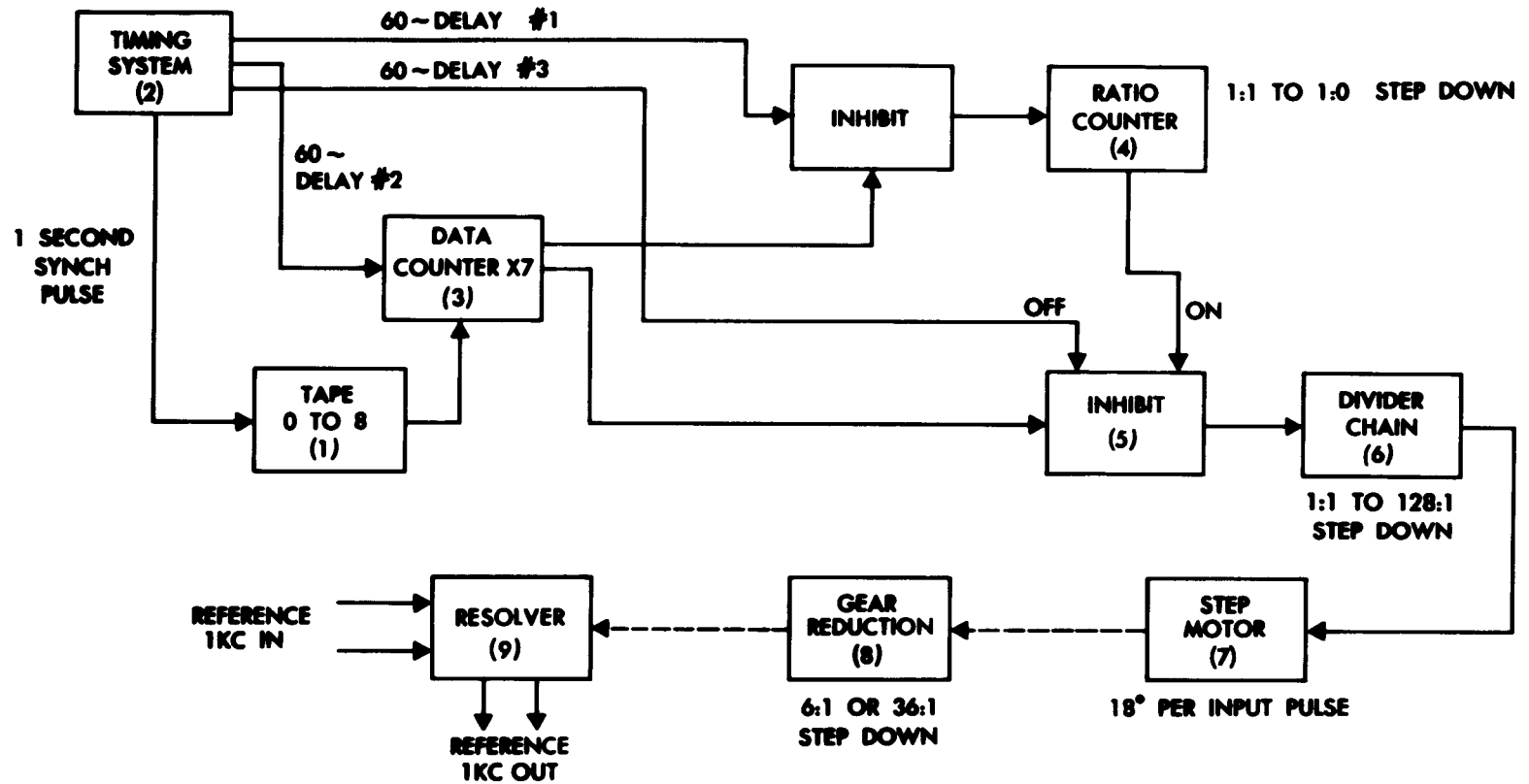

BLOCK DIAGRAM OF PHASE COMPENSATOR

FIG. 4.1

The fifth place differences change at most by eight digits for an increment of 15". Thus, sin 0° = 0, sin 15" = 0.000074. The tape is advanced one position each second of mean solar time, by a pulse from the timing system. At each position there is read out from the tape the sine difference value punched there, a number from zero to eight. This number is then sent to the data counter.

Timing system

The timing system consists of a 60 cycle per second time standard and associated pulse-forming circuitry. The timing system provides a one-second synchronizing pulse which reads out and advances the tape once a second. This is accomplished by a six stage binary counter which, once a cycle, by means of switching circuitry, has a count of 4 added to it. Thus the complete cycle is 60 counts instead of 64.

The timing system also provides three pulse sequences at the 60 cps repetition rate, synchronized with the one-second pulse, but with three different delays, achieved with RC delay networks and clamping diodes. These control the switching in various parts of the compensator.

The time standard is accurate to 5 parts in 10^7 per month. It is unaffected by line frequency variations.

Data counter

The data counter is the heart of the sine generation process. The one-second synchronizing pulse passes through the holes in the paper tape and reads a number into the data counter. The

gating is such that the number read into the counter is -7 times the number in the tape. Thus, a 2 becomes a -14. As soon as the data counter switching circuitry senses that its contents are not zero, the data counter begins to count at a 60 cps rate, meanwhile providing an output pulse for every input pulse from the timing system. When the contents of the data counter are again zero, i.e., when the number of input pulses from the timing system equals the number received from the tape, it stops and awaits the next input from the tape.

Thus, the data counter generates a train of pulses at a 60 cps rate equal in number to 7 times the number stored on the tape. At maximum rate of change of the sine wave, an 8 will appear on the tape, and during a 60-cycle second, the data counter will provide 56 pulses on the first 56 cycles.

Ratio counter

The ratio counter is a 14 stage binary counter which selects a pre-determined fraction of pulses from the data counter for removal. The first stage turns "on" for every other input pulse, the second stage turns on for every fourth input pulse, and so forth. Thus, the first stage can be gated to the inhibit circuit to remove one-half the input pulses, the second stage to remove one-fourth the input pulses, and so forth. This gating is accomplished with the use of fourteen switches which are set at calibration time. Any fraction F of the form

$$F = \sum_{j=1}^{14} \frac{\sigma_j}{2^j} \qquad \sigma_j = 0 \text{ or } 1$$

can be built up by setting the switches according to the σ_j's. If the j^{th} switch is in the off position, this switch will provide for the removal of $\frac{1}{2^j}$ of the input pulses.

Under consideration is the use of a ratio device such as this for a solar to sidereal time converter. By using enough stages, any desired accuracy could be obtained, such as one second per year.

Inhibit circuit

The inhibit circuit is where the actual pulse removal takes place. When the j^{th} position in the ratio counter goes on, and the j^{th} switch is off, a pulse from the ratio counter sets the inhibit trigger. After a delay, the pulse arrives from the data counter and is inhibited. Then after another delay, a pulse arrives to reset the inhibit trigger, which now awaits the next command from the ratio counter.

Divider chain

This is simply a seven-stage binary counter which reduces the pulse rate by $\frac{1}{2^n}$, where n can be selected by means of a rotary switch, from zero to seven. The number n is fixed for a given baseline such a value that, for a given total fraction of pulses removed, a minimum fraction is removed in the ratio counter and a maximum fraction in the divider chain.

Step motor, gear reduction, resolver

These are self-explanatory. The stepping motor rotates 18° per input pulse. This is stepped down by 36:1 to 0.5° per input pulse by the gear train, which in turn rotates the resolver.

Setting the compensator for a particular set of parameters

This is best illustrated with an example. The amplitude of the reference sine wave which is to be subtracted from the phase sine wave of the received signal is $\frac{2\pi d}{\lambda} \cos \delta \sin \gamma$, in units of radians. Assume the following parameters:

$$\frac{2\pi d}{\lambda} = 189.46$$

$$\delta = \cos^{-1} (0.92) \cong 23°$$

$$\gamma = \xi = \pi/2$$

Therefore the amplitude is

$$\frac{2\pi d}{\lambda} \cos \delta \sin \gamma = 174.3 \text{ radians} = 10{,}000 \text{ degrees.}$$

This means that during the course of six hours from mean noon during which the hour angle has increased by 90° and the phase sine wave has gone from zero to full amplitude, the motor must receive 20,000 pulses, since it advances 0.5° per pulse. The data counter, on the other hand, during this same period generates a sequence of pulses equal to 7×10^5. Thus, a reduction of $\frac{2}{70}$ is called for. This reduction can be written

$$\frac{1}{32} \times \frac{32}{35}$$

The reduction of $\frac{1}{32}$, called the coarse adjustment, is set by tapping off the output of the fifth stage of the divider chain.

The ratio of $\frac{32}{35} = .914286$ is set in the ratio counter. The ratio counter can be set to inhibit any number of input pulses during the course of its $2^{14} = 16,384$ count cycle. The exact number we would like to pass is

$$\frac{32}{35} \times 16,384 = 14,979.7$$

But, since we can pass only an integral number of pulses, we must be content with 14,980. Thus, the true ratio will be

$$\frac{14,980}{16,384} = .914307$$

The error is $\frac{.3}{14,979.7} \sim .00002$

To set the ratio counter to pass the 14,980 pulses, first write the number less one in binary form as follows:

$$14,979 = 11101010000011$$

Then, if the binary digits are thought of as stages of the ratio counter, all stages with a 1 should be in the on (not inhibit) position. The maximum error is

$$\frac{0.5}{\text{Number of counts passed}}$$

The greater the number of counts, the smaller the percent error. The divider chain permits the passing of greater than $\frac{1}{2} \times 16,384$ pulses. Thus, the greatest error is of the order of .00006.

Phase compensator error

The phase of the 1 kc signal input to the phase meter is equal to the phase difference between the receiving antennas.

From (4.1) the phase of the 1 kc signal for an east-west baseline (where γ and $\xi = \pi/2$) is given by

$$4.3 \qquad \phi_{sig} = \frac{2\pi d}{\lambda} \sin HA_o \cos \delta_o$$

Taking into account a change in declination equal to $\Delta\delta_o$ over a 24-hour period, and with the time t given in hours, (4.3) becomes

$$4.4 \qquad \phi_{sig} = \frac{2\pi d}{\lambda} \cos \left(\delta'_o + \frac{\Delta\delta_o t}{24}\right) \sin HA_o$$

where δ'_o is the declination of the center of the sun at t = o.

Prior to calibration, the compensator inserts a nearly identical time-varying phase into the reference signal input to the phase meter. Since the amplitude of the phase sine wave output from the compensator can be varied only in fixed increments an error results from the fact that the preset amplitude differs from that required. It will be shown shortly that this error can be considered to be equivalent to an angular declination setting error δ_e. The phase compensator reference signal is given by

$$4.5 \qquad \phi_{ref} = \frac{2\pi d}{\lambda} \cos (\delta'_o + \delta_e) \sin (HAMS)$$

where HAMS is the hour angle of the mean sun.

The system is calibrated so that at transit (t = 0) the origin of the compensator sine wave is coincident with the origin of the sine wave resulting from the motion of the sun. The rate of change of the compensator sine wave is synchronized to the mean sun (HAMS) since the timing input to the compensator system is derived from mean solar time. Thus from (4.5), one obtains

$$4.6 \qquad \phi_{ref} = \frac{2\pi d}{\lambda} \cos (\delta'_o + \delta_e) \sin (HA_o - \frac{\Delta Et}{24})$$

where δ'_o = the declination of the sun at t = 0

HA_o = the hour angle of the apparent sun

ΔE = change in the equation of time over the following 24-hour period.

A straight line approximation is used in the determination of the change in declination and the variation in position of the apparent sun with respect to the mean sun. The declination error δ_e is related to the fractional error η in the amplitude of the compensator phase sine wave by

$$4.7 \qquad \eta = \frac{\cos \delta'_o - \cos (\delta'_o + \delta_e)}{\cos \delta'_o}$$

Assuming that δ_e is small and solving for δ_e in terms of δ'_o we have

$$4.8 \qquad \delta_e = \sqrt{\tan^2 \delta'_o + 2\eta} - \tan \delta'_o$$

It was shown that using 14 binary stages in a binary divider results in a maximum possible error of $\eta = 1/2^{14} = 1/16,384$. Table 4.1 lists the resulting δ_e for $\eta = 1/2^{14}$ for different solar declination angles.

δ'_o	δ_e (minutes)
0°	38.0
1°	11.2
2.5°	4.7
5°	2.4
10°	1.16
15°	.79
20°	.583

TABLE 4.1

The phase error is the difference in phase between that which is inserted by the compensator and the signal phase. From 4.4 and 4.6 this phase difference is

$$4.9 \qquad \Delta\phi = \frac{2\pi d}{\lambda}\left[\cos\left(\delta'_o + \frac{\Delta\delta_o t}{24}\right)\sin HA_o - \left(\cos(\delta'_o+\delta_e)\sin\left(HA_o - \frac{\Delta Et}{24}\right)\right)\right]$$

Assuming that over any one observation period the change in the equation of time and declination is small, Equation (4.9) becomes

$$4.10 \qquad \Delta\phi = \frac{2\pi d}{\lambda}\left\{\sin HA_o\left[\cos\delta'_o\left(\frac{1}{2}\left(\frac{\Delta Et}{24}\right)^2 - \frac{1}{2}\left(\frac{\Delta\delta_o t}{24}\right)^2\right) - \frac{\Delta\delta_o t}{24}\sin\delta'_o\right] + \frac{\Delta Et}{24}\cos HA_o \cos(\delta'_o + \delta_e)\right\}$$

The phase error given in Equation (4.9) is the electrical phase shift which will be evidenced at the output of the phase meter resulting from the error caused by a change in declination and equation of time over the period of observation. As an example, the accumulated error over a two-day period is given in Figure 4.2. Plotted along the ordinate is the phase shift in radians.

Consider for example a 100λ baseline. After 24 hours, on January 1, the phase error is almost $4\pi \times 10^{-1}$ radians or 72 degrees. The phase shift of 72 degrees would also result if the position of the sun were to shift by about 7 minutes of arc in an east-west direction at transit.

From Equation (4.10) and Figure 4.2 it is clear that at transit following n days of operation the accumulated error is simply

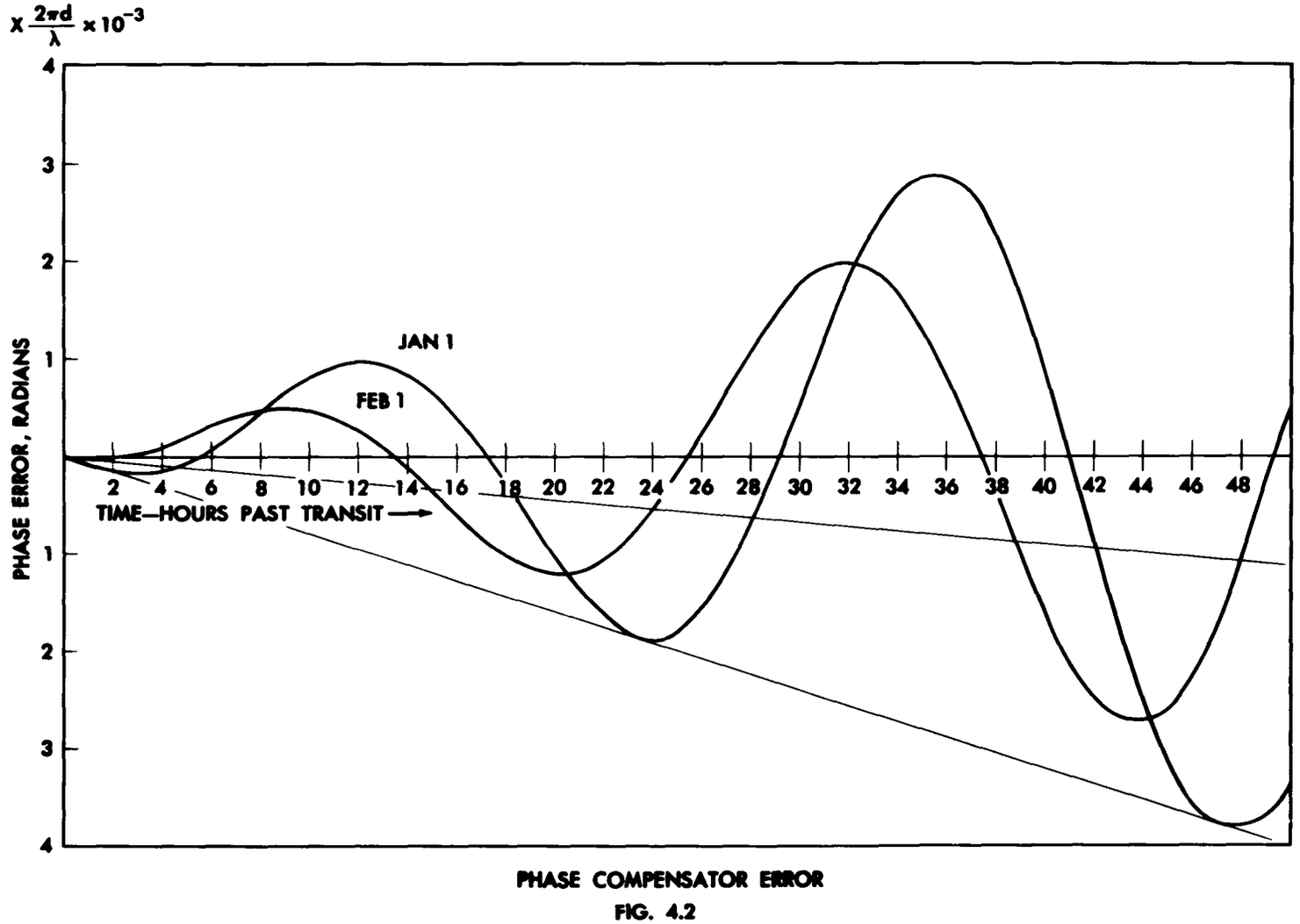
$X \frac{2\pi d}{\lambda} \times 10^{-3}$
PHASE ERROR, RADIANS
4
3
2
1
1
2
3
4
JAN 1
FEB 1
2 4 6 8 10 12 14 16 18 20 22 24 26 28 30 32 34 36 38 40 42 44 46 48
TIME—HOURS PAST TRANSIT
PHASE COMPENSATOR ERROR

FIG. 4.2

$\frac{2\pi d}{\lambda} n\Delta E \cos(\delta_o' + \delta_e)$ or approximately equal to $\frac{2\pi dn\Delta E}{\lambda} \cos \delta_o'$. Thus, for quick reference the error at successive transits is easily determined. The straight lines plotted in Figure 4.2 run through the transit error points.

The variation of the error phase curve plotted for $\eta = 0$ and $\eta = \frac{1}{2^{14}}$ (maximum error in δ_e) is shown in Figure 4.3 for the solar coordinate parameters of March 2. Since η is precisely known for a given set of data, the precise corrections can be made for this error in the phase compensator. A simpler solution, however, is to make η smaller by adding additional binary stages in the ratio counter if the additional precision is required.

Phase compensator calibration

In practice the accumulated phase error is limited by routine calibration of the compensator. The origin and amplitude of the compensator phase sine wave are changed at the time of calibration to account for the change of the equation of time and the change in the declination of the optical sun respectively which have occurred following the previous calibration.

The origin of the sine wave stored on the paper tape is shifted to coincide with the origin of the sine wave resulting from the motion of the apparent sun. This is accomplished by moving the tape ahead or behind in step increments, the amount determined by the change in the equation of time since the last calibration. The appropriate change in the phase amplitude is accomplished by setting a bank of 14 switches which control the ratio counter to a predetermined setting.

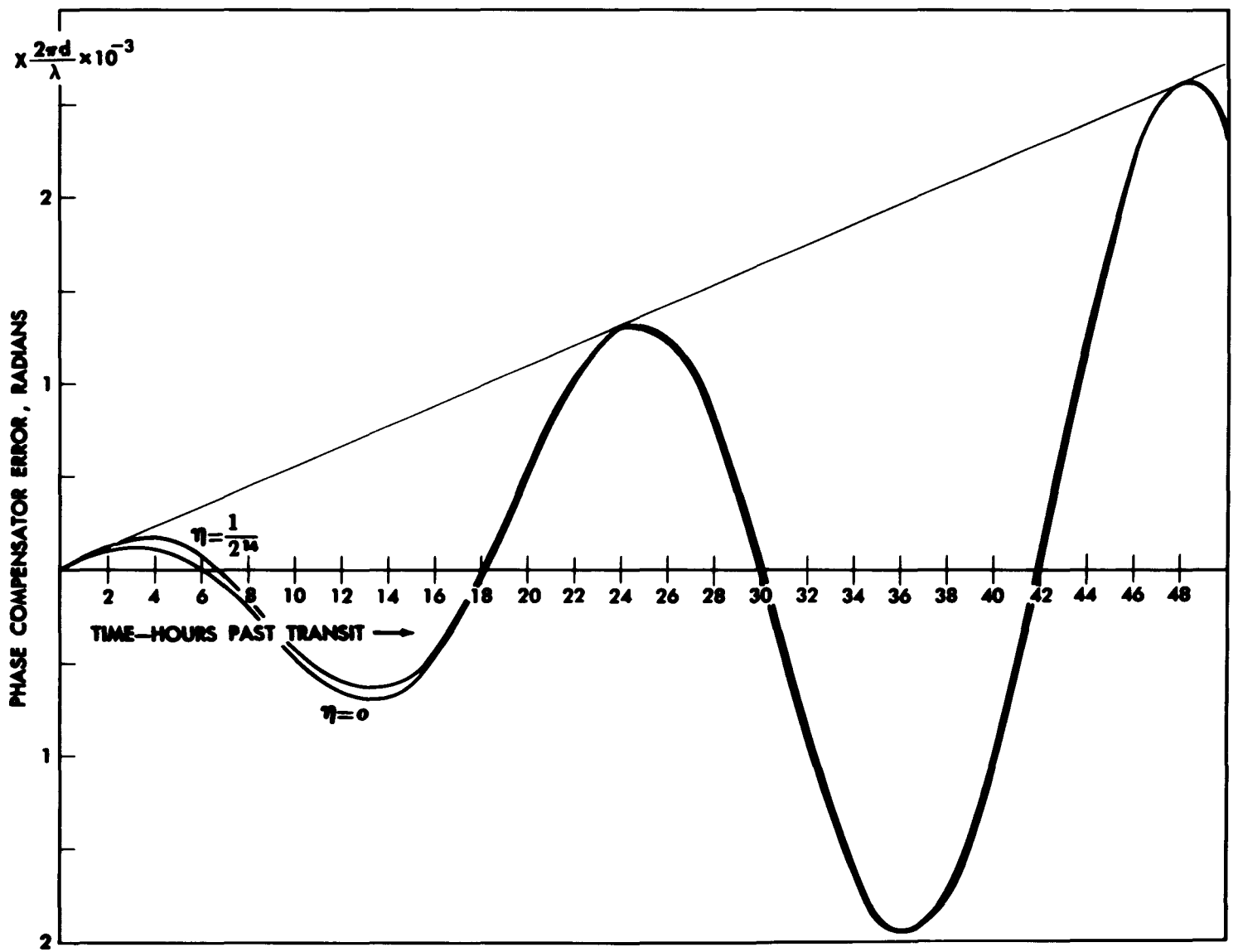

VARIATION OF COMPENSATOR ERROR

FIG. 4.3

The accumulated phase error as a function of time is known from equation (4.9). The accumulated phase error since the previous calibration is removed from the system by subtracting a phase equal to the accumulated phase error using a manually operated resolver.

PART V

THE EFFECT OF AN EXTENDED SOURCE DIMENSION AND FINITE RECEIVER BANDWIDTH ON THE RECEIVED POWER

In the discussion to follow, the available power is defined as the power input to the interferometer system. The term "effective power" refers to the component of the available power which results in a lobe sweep signal component. The effective power is reduced if the source dimension is not small compared to the lobe separation of the antenna pattern. A further reduction is realized in the event of a finite receiver bandwidth which results from the fact that the phase difference between the two antennas varies over the pass-band of the receiver.

This section reviews the general problem of determining the effective power. The effect of a finite source size is first investigated in which the fringe blurring due to a finite receiver bandwidth is considered negligible. The combined effects of both bandwidth and finite source dimension are presented graphically to provide a quantitative illustration of the relative importance of the two effects. A detailed analytical proof of the relations presented in this section is given in Appendix B.

Extended source with zero receiver pass-band

It was first shown by McReady, Pawsey, and Payne-Scott (19) and is proven in Appendix B that the effective power is given by a Fourier sine and cosine transform of the brightness distribution of the source.

Given a brightness distribution symmetrical about a given incident angle it is shown in Appendix B that the lobe sweep modulation is given by the relation

$$5.1 \qquad S(t) = \cos\left(\omega_a t + \frac{2\pi d}{\lambda} \sin\theta_o + \phi_a\right) \int_{-\Delta\theta}^{+\Delta\theta} P(\theta',t) \cos(A\theta')\, d\theta'$$

where θ = incident angle

$A = \frac{2\pi d}{\lambda} \cos\theta_o$

θ' = angle measured from source position θ_o

ω_a = lobe sweep frequency

$\Delta\theta$ = source half width

$P(\theta',t)$ = brightness distribution of the source

From (5.1) the amplitude of the modulation component for a symmetrical, time invariant brightness distribution is given by

$$5.2 \qquad \overline{S(A)} = 2 \int_0^{\Delta\theta} P(\theta') \cos(A\theta')\, d\theta'$$

The modulation component for a circular source with radial symmetry from Appendix B is given by

$$5.3 \qquad \overline{S(A)} = 2\pi \int_0^R P(r)\, J_o(Ar)\, r\, dr$$

In the special case of a uniform circular source we have

$$5.4 \qquad \overline{S(A)} = \frac{P\pi R^2 2J_1(AR)}{AR}$$

J_o and J_1 are Bessel functions.

It is thus clear from the transform relations given that the received amplitude of the lobe sweep signal is related to an integral of the brightness distribution. Since an infinite number of assumed brightness distributions will result in the same output $\overline{S(A)}$, it is necessary to obtain measurements of the received effective power for several baselines to determine the actual brightness distribution of the source. It is necessary to restrict observations to source positions near normal incidence or to insert cable delays in the transmission lines for large incident angles to avoid the necessity of correcting for errors resulting from a finite receiver bandwidth.

Uniform rectangular distribution

Evaluating the integral relationship given in (5.1) for the special case of a uniform, rectangular, and time invariant brightness distribution at normal incidence, the modulation component is given by Equation (5.5). The factor $\Delta\theta$ is the source half-width.

$$5.5 \qquad S(t) = 2P\Delta\theta \cos(\omega_a t + \phi_a) \frac{\sin \frac{2\pi d\Delta\theta}{\lambda}}{\frac{2\pi d\Delta\theta}{\lambda}}$$

From Equation (5.5) it is clear that for a fixed source width the amplitude of the modulation component falls off as the antenna separation (d) is increased and vanishes at $d = \frac{\lambda}{2\Delta\theta}$. A small increase in d above this point will result in an increase in S(t) with a 180 degree reversal in the phase. In the limit for large values of d, S(t) will fall to zero.

Up to this point the discussion has been concerned with the

effective power which will result in a modulation component. In practice the intensity recordings are equal to the magnitude of S(t), i.e., $\overline{S(A)}$, multiplied by the gain constant of the system. Since the evaluation of source dimension depends on the determination of the variation of the received power with baseline, several measurements of intensity must be made at different baseline separations. It is clear that gain variations during the measurements must be minimized if this technique of source determination is to be useful.

In a total-power interferometer the depth of the interference pattern is measured by taking the ratio of the minimum to maximum of the recorded response as the source passes through the interference fringes. From (20) it is shown that this ratio at normal incidence for a rectangular source distribution is given by

$$5.6 \qquad R = \frac{1 - \dfrac{\sin \frac{2\pi d \Delta\theta}{\lambda}}{\frac{2\pi d \Delta\theta}{\lambda}}}{1 + \dfrac{\sin \frac{2\pi d \Delta\theta}{\lambda}}{\frac{2\pi d \Delta\theta}{\lambda}}}$$

Thus, from a single measurement of the minimum and maximum, the source dimension for a rectangular distribution can be unambiguously determined in a total power system. In the event the internal system noise is large compared to the effective noise power, the total power technique has severe limitations.

Point source with finite receiver pass-band

From Appendix B it was shown that the effective power received by an interferometer system for a point source and a system bandwidth Δf is given by

$$5.7 \qquad \bar{S} = \text{available power} \times \frac{\sin\left(\frac{\pi n \Delta f}{f}\right)}{\frac{\pi n \Delta f}{f}}$$

The factor n is the path difference in wavelengths between the two antennas. As an illustration consider a 2 mc bandwidth at an operating frequency of 200 mc. For a path difference of 60 wavelengths the effective power from (5.7) is reduced by approximately a factor of two.

<u>An illustration of the combined effects of receiver bandwidth and source diameter</u>

Figure 5.1 is a three-dimensional set of curves showing the effective power relative to a point source and zero receiver bandwidth as a function of bandwidth and source diameter. A rectangular pass band and a uniform circular source distribution are assumed. The other parameters are constant as indicated. The curves were calculated by numerically integrating Equation (B6) of Appendix B with respect to frequency.

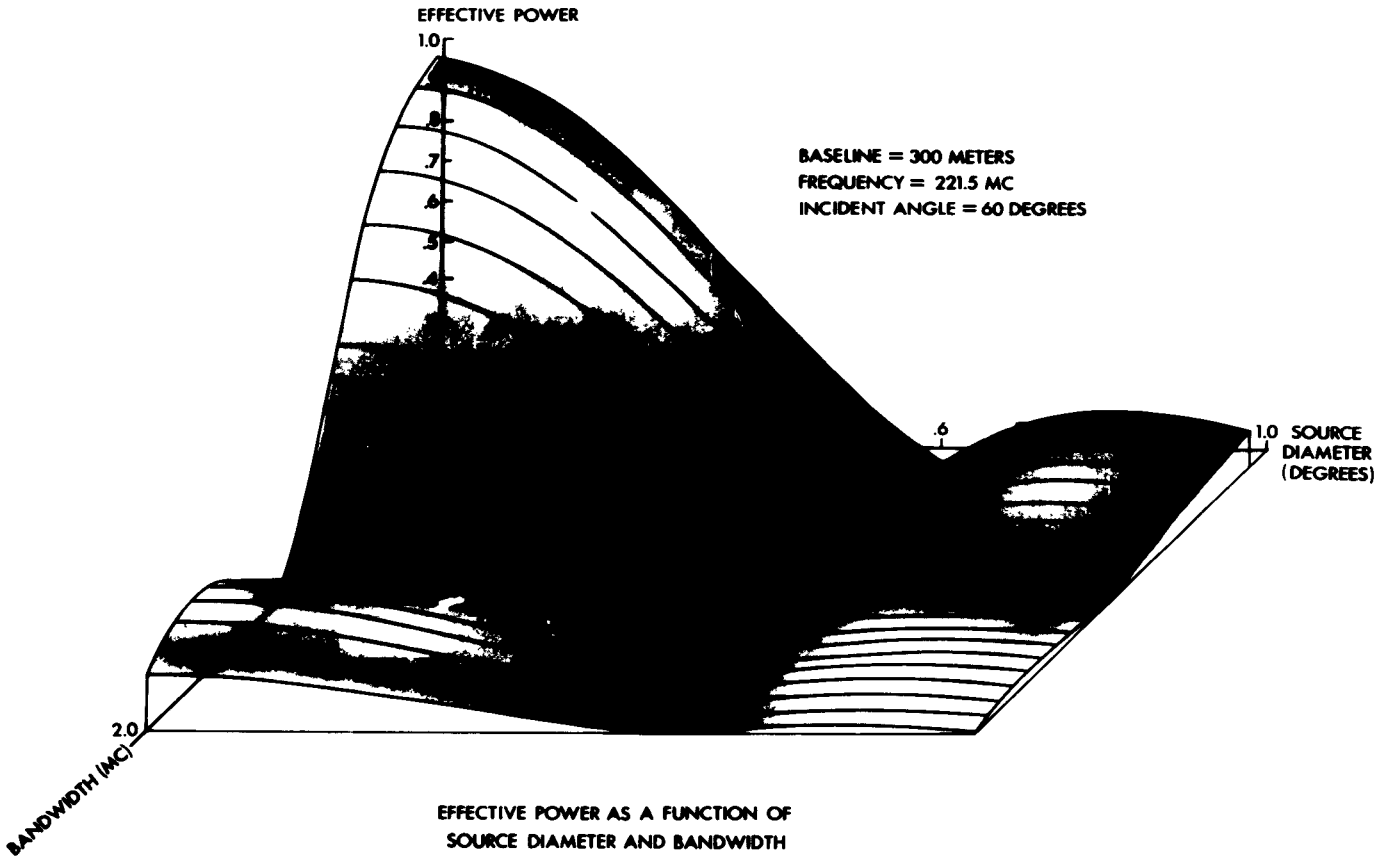

EFFECTIVE POWER AS A FUNCTION OF SOURCE DIAMETER AND BANDWIDTH

FIG. 5.1

PART VI

DISCUSSION OF ERRORS

The following errors relating to the measurement of burst positions will be discussed:

1 - deviation of center frequency

2 - atmospheric refraction

3 - ionospheric scintillation

4 - internal phase variations

5 - transient response

6 - ground reflections

7 - baseline orientation and antenna separation

1. Deviation in center frequency

A deviation in center frequency may occur due to local oscillator drift or a change in filter or tuned circuit characteristics.

1A. Error in position measurements relative to the radio center of the sun due to a shift in center frequency

Consider a burst which is displaced an angle $\Delta\theta$ from the radio center of gravity which is located at an incident angle θ_o. The phase angle of the burst measured with the interferometer system is determined from the recorded measurements using equation (3.10). This equation gives the relationship between the phase of the burst and the total change of received signal amplitude and phase resulting from the superposition of the burst and preburst solar noise power components. The phase angle of the radio center of gravity is

$$\phi_{cg} = \frac{2\pi d}{\lambda} \sin \theta_o$$

The phase angle of the burst is

$$\phi_b = \frac{2\pi d}{\lambda} \sin (\theta_o + \Delta\theta) \cong \frac{2\pi d}{\lambda} (\sin \theta_o + \Delta\theta \cos \theta_o)$$

The measured phase angle of the burst relative to the radio center is therefore

6.1 $$\Delta\phi = \phi_b - \phi_{cg} = \frac{2\pi d}{\lambda} \Delta\theta \cos \theta_o \cong \frac{2\pi d}{c} f\Delta\theta \cos \theta_o$$

In the calculation of the burst position from the measurements the operating frequency is considered fixed and equal to f_o. From equation (3.15), the calculated burst position r for a measured phase shift $\Delta\phi$ rewritten to show frequency explicitly is

6.2 $$r = \frac{c\Delta\phi}{2\pi d\, f_o \cos \theta}$$

If at the time of measurement the operating frequency is in reality not f_o but $f_o + \Delta f$ the burst position, from the measurements and calculations of (6.1) and (6.2), are

6.3 $$r_{calc} \cong \frac{\Delta\theta\ (f_o + \Delta f)}{f_o}$$

The actual burst position, however, was defined to be at $\Delta\theta$. The error relation to the radio center of gravity is therefore

6.4 $$\Delta f = r_{actual} - r_{calc} \cong \Delta\theta \left[1 - \frac{f_o + \Delta f}{f_o}\right] = -\frac{\Delta\theta\Delta f}{f_o}$$

Thus, at 200 mc a 2 mc error in the center frequency will result in an error of only one percent in relative position measurements. Since the bandwidth of the system is only approximately 600 kc this error will be small and can generally be disregarded.

1B. Error in absolute position measurements resulting from a deviation in the center frequency

Consider the sun to be a circular, symmetrical radio source. Assuming that no phase errors exist in the interferometer system, the electrical phase shift occurring at the output of the phase meter will vary with the incident angle θ, and is given by

$$6.5 \qquad \phi = \frac{2\pi d \sin\theta}{\lambda} = \frac{2\pi f d}{c} \sin\theta$$

A shift in the operating frequency to $f_o + \Delta f$ will result in a change in the electrical phase angle given by

$$6.6 \qquad \Delta\phi = \phi(f_o + \Delta f) - \phi(f_o) = \frac{2\pi d \Delta f}{c} \sin\theta$$

Assuming that the position error resulting from a frequency shift is small, the position of the source, based on the measured phase, with respect to the true position is given by (3.15) and is

$$6.7 \qquad r = \frac{\lambda_o}{2\pi d} \frac{\Delta\phi}{\cos\theta}$$

Substituting (6.6) the resultant error is

$$6.8 \qquad r = \frac{\Delta f}{f_o} \tan\theta$$

It is seen that the absolute measurement error can be appreciable and must be considered for large incident angles. For example, given $\Delta f = 10$ kc, $f_o = 200$ mc, $\theta = 85°$, the resulting error in the absolute measurement of source position is approximately 2 minutes of arc.

2. Atmospheric refraction errors

A. Low elevation angles

Tropospheric and ionospheric refraction both increase with a decrease in elevation angle. McReady, Pawsey and Payne-Scott (19), comparing a theoretical model with measurements of the position of the sun at 200 mc, have shown that at an elevation angle of 10 degrees the tropospheric refraction is approximately 9 minutes of arc. Ionospheric refraction has been investigated by Payne-Scott and McReady (21) and Bailey (22). On the basis of this early work it has been estimated (23) that the ionospheric refraction is expected to be typically 5 minutes of arc or less at 200 mc. Since the two types of refraction oppose each other the net error will be less than the individual errors.

B. High elevation angles

Smith (24) was the first to note that a horizontal gradient in the total electron content can result in an apparent shift in the right ascension of a source at transit. From experimental observations of several sources near transit, Smith observed that the maximum regular change in right ascension was 0.5 minutes of arc at 81.5 mc. Since the angle deviation resulting from this type of "wedge" refraction varies with the square of the wavelength the expected angular error at 221 mc from this effect should be comparatively small.

3. Ionospheric scintillation errors

From studies made of the scintillation in the received power from discrete radio sources it has been demonstrated that the

observed fluctuations are probably due to localized inhomogeneities in the ionosphere. The scintillation amplitude is found to increase with a decrease in elevation, and vary approximately with the square of the operating wavelength. The rms short term angle fluctuations about the position of a radio star at 8 meters wavelength for elevation angles 60 degrees or higher has been reported by Hewish (25) to be 5 minutes of arc. Slow irregular angular variations in the relative position of the discrete source Cygnus have been reported by Lawrence, Jespersen and Lamb (26) to be commonly 0.5 degrees at 53 mc. Assuming an inverse square relation between the magnitude of the scintillation and the frequency the angular deviation at 221 mc is expected to be typically 1-2 minutes of arc in the majority of circumstances. For a review of the work done on scintillations the reader is referred to a paper by Booker (27).

It is generally assumed that the origin of the irregularities responsible for the scintillations is in the F region. The sun's subtended angular dimension is of the same order as that of the estimated scale of the irregularities. A source dimension of this size will result in greatly smearing out the effects of scintillation over that occurring from a point source. It is therefore expected that the enhanced active regions on the sun will be more prone to scintillation effects than the component originating from the comparatively large quiet sun.

4. Errors resulting from internal phase variations

The lobe sweep system employs a technique which measures the phase difference between two rf signals. Any variation in the

phase difference between the two signals prior to square law detection will result in an apparent shift in the incident angle that the source makes with the antenna baseline. The differential phase shift between the two antenna cables and local oscillator lines needs to be considered. Variation of the phase difference between the two signals separated by the 1 kc lobe sweep frequency in the common IF amplifier is an additional factor that should be considered.

Small shifts in the 1 kc reed oscillator which control the lobe sweep frequency could introduce phase shifts in the system. An additional factor to be considered is the variation of phase difference between the two signals resulting from the AGC function of the IF amplifier, i.e., phase shifts as a function of the gain setting of the amplifier. The analog phase meter must measure the phase difference independent of the amplitude of the input signals to obtain meaningful data.

An experimental measurement of all those factors combined which tend to introduce phase errors, exclusive of the error resulting from differential phase shifts in the antenna cables, has established that the system is capable of measuring the electrical phase difference to within an accuracy of about ± 7 electrical degrees. The long term stability measured independent of errors introduced by the phase meter was found to be ± 3.5 degrees over 7 days. At transit an uncertainty in the electrical phase angle of $\Delta\phi$ will result in an uncertainty in the incident angle $\Delta\theta$ given by

$$6.9 \qquad \Delta\theta = \frac{\lambda \Delta\phi}{2\pi d}$$

Thus for an antenna separation of 50λ and an uncertainty of electrical phase angle of 5 degrees the corresponding uncertainty in measurement of source position near normal incidence is approximately 1 minute of arc.

5. Transient response errors

The determination of source position using the Boeing system depends on two independent measurements, the total intensity and phase. From a knowledge of the composite power and phase before and during the burst and assuming superposition the phase shift and hence the position of a burst is calculated using the method outlined in Part III.

From Appendix A it was shown that the phase shift of a burst is related to the measured quantities by

$$6.10 \qquad \Delta\phi = \tan^{-1} \frac{(P_2/P_1) \sin \Delta\chi}{(P_2/P_1) \cos \Delta\chi - 1}$$

where P_2/P_1 is the measured power increase during the burst

$\Delta\chi$ is the total measured phase shift variation caused by the burst.

For the case where the intensity recording is a logarithmic function of the burst intensity, and the recording time constants of the intensity and phase recordings are the same and equal to τ, it can be shown that the measured phase as a function of time, for a burst of constant relative amplitude P_2/P_1 and duration t is given by

$$6.11 \qquad \Delta\phi(\text{measured}) = \tan^{-1} \frac{(P_2/P_1)^{(1-e^{-t/\tau})} \sin[\Delta\chi(1-e^{-t/\tau})]}{(P_2/P_1)^{(1-e^{-t/\tau})} \cos[\Delta\chi(1-e^{-t/\tau})] - 1}$$

The error in the determination of the electrical phase shift of the burst as a function of the total received increase in power from (6.10) is plotted in Figure 6.1 for burst durations from $.2\tau$ to 1.6τ. The error shown is the percentage error in the determination of the phase shift of the burst resulting from the finite response of the system. The true phase shift $\Delta\phi$ will be greater than that determined from the measurements by the indicated percentage error. If no corrections for transient errors are applied in the determination of the burst positions, it seen that for short duration bursts of equal duration less intense bursts will produce a greater phase shift and hence greater measured position deviations relative to that produced by more intense bursts.

It is therefore concluded that when transient delays are important it is required to apply a correction which is a function of both the increase in power level and the duration of the burst. A special circuit has been designed which will provide an analog presentation of the duration of the bursts received. Successful operation of this device will enable the necessary data to be obtained for transient response correction without having to resort to fast chart speeds.

6. and 7. <u>Errors from ground reflections and baseline orientation and antenna separation</u>

The received signal at each interferometer antenna is the superposition of the direct and ground reflected signal. The

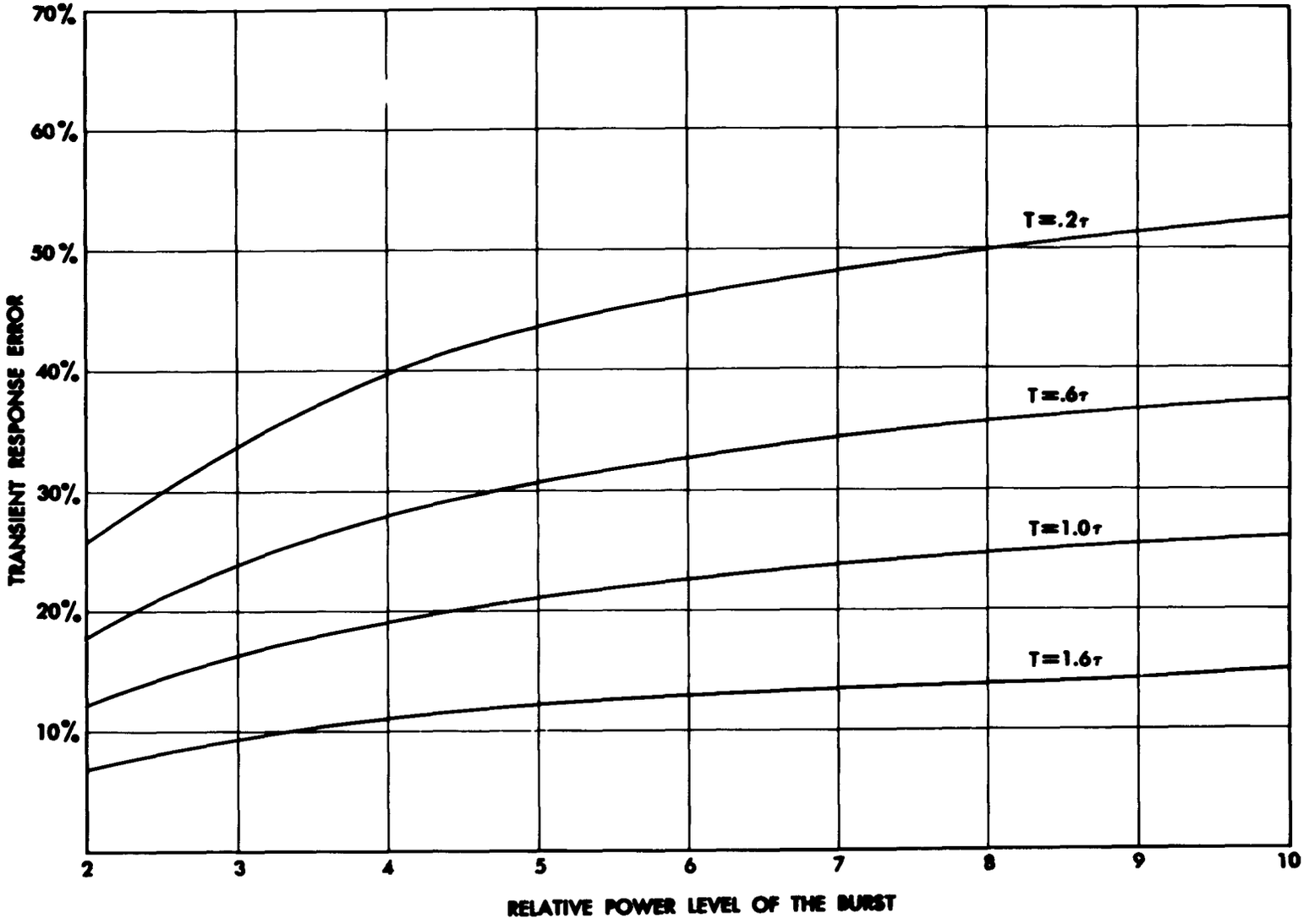

TRANSIENT RESPONSE ERROR
FIG. 6.1

phase meter provides a measure of the path difference of this composite received signal between the two antennas. It is therefore apparent that variations in the ground reflected path between the two antennas will result in extraneous phase variations as measured at the output of the phase meter. These irregular slowly varying phase anomalies should nearly repeat themselves on a day-to-day basis, but will gradually change due to the change in declination of the sun. It was pointed out in Part IV that the total phase shift of the signal between the receiving antennas will show up as a sine wave variation, the phase and amplitude of which are determined by the baseline orientation and separation of the antennas.

In using the phase compensator the output of the phase meter represents the difference between the predicted and the actual phase shift in the system. Such a measured phase difference is either a result of a shift in the center of gravity of the radio center from the optical center or a result of ground reflections and errors related to baseline orientation and antenna separation. By repeated observations of the resulting errors it is expected that it will be possible to separate and evaluate those due to ground reflections and those due to baseline orientation and antenna separation.

APPENDIX A

CALCULATION OF BURST PARAMETERS FROM INTERFEROMETER DATA

Let the received signal before the occurrence of the burst be

$$P_1 \cos (\omega_a t + \chi_1)$$

Let the received signal after the burst be

$$P_2 \cos (\omega_a t + \chi_2)$$

Let the component due to the burst be denoted as

$$P_x \cos (\omega_a t + \chi_x)$$

Since linear superposition applies, it follows that

$$P_2 \cos (\omega_a t + \chi_2) = P_1 \cos (\omega_a t + \chi_1) + P_x \cos (\omega_a t + \chi_x) \tag{A1}$$

It is desired to find P_x and χ_x. P_1, χ_1, P_2, and χ_2 are the observables.

Expanding Eq. (A1) into components of sin $\omega_a t$ and cos $\omega_a t$ gives the pair of equations:

$$P_1 \cos \chi_1 + P_x \cos \chi_x = P_2 \cos \chi_2 \tag{A2}$$

$$P_1 \sin \chi_1 + P_x \sin \chi_x = P_2 \sin \chi_2 \tag{A3}$$

Therefore,

$$\tan \chi_x = \frac{P_2 \sin \chi_2 - P_1 \sin \chi_1}{P_2 \cos \chi_2 - P_1 \cos \chi_1}$$

Let $\chi_x - \chi_1 = \Delta\phi$ (source displacement)

$\chi_2 - \chi_1 = \Delta\chi$ (signal displacement)

Then

$$\tan \Delta\phi = \frac{(P_2/P_1) \sin \Delta\chi}{(P_2/P_1) \cos \Delta\chi - 1}$$

To find the magnitude P_x of the burst, write Eqs. (A2) and (A3) as

$$P_x \cos \chi_x = P_2 \cos \chi_2 - P_1 \cos \chi_1 \tag{A5}$$

$$P_x \sin \chi_x = P_2 \sin \chi_2 - P_1 \sin \chi_1 \tag{A6}$$

Squaring both sides and adding gives

$$P_x^2 = P_2^2 + P_1^2 - 2P_1P_2 \cos (\chi_2 - \chi_1)$$

or finally,

(A7) $$P_x = \sqrt{P_1^2 + P_2^2 - 2P_1P_2 \cos \Delta\chi}$$

APPENDIX B

THE FOURIER TRANSFORM RELATIONSHIPS FOR THE ENERGY DISTRIBUTION ACROSS THE SOLAR DISC

Given two antennas A and B on an interferometer baseline, with incident phases ϕ_x and ϕ_y respectively, the received signal for a lobe-sweep system is proportional to

$$P \cos (\omega_a t - \phi_x + \phi_y + \phi_a)$$

where P is the effective power at the antenna terminals, and the designations A and B are selected such that the phase at A subtracts. The factor ω_a is the lobe-sweep angular frequency. The angle ϕ_a is a phase constant of the system. The quantity $\phi_y - \phi_x$ is dependent on the incident angle θ between the incident ray and the normal plane to the baseline (Fig. B1).

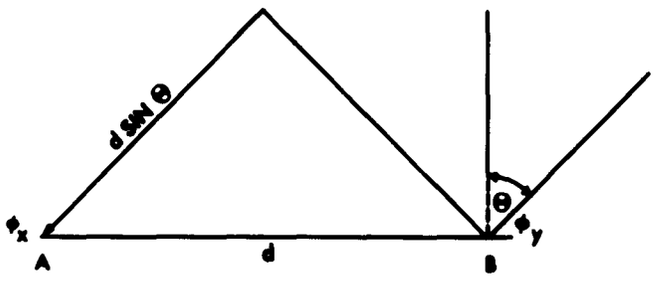

$$\phi_y - \phi_x = \frac{2\pi d}{\lambda} \sin \theta$$

INTERFEROMETER GEOMETRY
FIG. B1

For a source at incident angle θ, the received signal, S, is $P \cos (\omega_a t + \phi_a + \frac{2\pi d}{\lambda} \sin \theta)$.

If the source intensity varies with time, and is distributed over all incident angles, then the received signal becomes

(B1) $$S(t) = \int P(\theta, t) \cos\left(\omega_a t + \phi_a + \frac{2\pi d}{\lambda} \sin\theta\right) d\theta$$

where $P(\theta,t)$ is the intensity distribution.

The case of special interest is the one where the integration is over a short range in θ as

$$\sin\theta \cong \sin\theta_o + (\theta - \theta_o)\cos\theta_o$$

In this case the integration becomes

(B2) $$S(t) = \int P(\theta,t)\cos\left(\omega_a t + \phi_a + \frac{2\pi d}{\lambda}\left[\sin\theta_o - \theta_o\cos\theta_o\right] + \frac{2\pi d}{\lambda}\theta\cos\theta_o\right) d\theta$$

Let $$\alpha = \omega_a t + \phi_a + \frac{2\pi d}{\lambda}(\sin\theta_o - \theta_o\cos\theta_o)$$

$$A = \frac{2\pi d}{\lambda}\cos\theta_o$$

Then

(B3) $$S(t) = \cos\alpha \int P(\theta,t)\cos A\theta\, d\theta - \sin\alpha \int P(\theta,t)\sin A\theta\, d\theta$$

<u>Symmetrical distribution</u>

In the event that the distribution is symmetrical around the center value θ_o, the result reduces to a simpler form:

$$S(t) = \int P(\theta,t)\cos\left[\omega_a t + \phi_a + \frac{2\pi d}{\lambda}\sin\theta_o + \frac{2\pi d}{\lambda}\cos\theta_o(\theta-\theta_o)\right] d\theta$$

$$= \cos\left(\omega_a t + \phi_a + \frac{2\pi d}{\lambda}\sin\theta_o\right)\int P(\theta,t)\cos\left[\frac{2\pi d}{\lambda}(\cos\theta_o)(\theta-\theta_o)\right] d\theta$$

$$- \sin\left(\omega_a t + \phi_a + \frac{2\pi d}{\lambda}\sin\theta_o\right)\int P(\theta,t)\sin\left[\frac{2\pi d}{\lambda}(\cos\theta_o)(\theta-\theta_o)\right] d\theta$$

If the distribution is symmetrical, then the second integrand is odd around $\theta-\theta_o$ and vanishes. We are left with

$$S(t) = \cos\left(\omega_a t + \phi_a + \frac{2\pi d}{\lambda}\sin\theta_o\right) \int_{\theta_o-\Delta\theta}^{\theta_o+\Delta\theta} P(\theta,t)\cos\left[\frac{2\pi d}{\lambda}(\cos\theta_o)(\theta-\theta_o)\right] d\theta$$

Let $\theta-\theta_o = \theta'$. Then

(B4) $$S(t) = \cos\left(\omega_a t + \phi_a + \frac{2\pi d}{\lambda}\sin\theta_o\right) \int_{-\Delta\theta}^{+\Delta\theta} P(\theta',t)\cos\left[\frac{2\pi d}{\lambda}(\cos\theta_o)\theta'\right] d\theta'$$

Change to polar coordinates

Suppose the distribution is an area distribution, specified by the angle θ and another axis orthogonal to it. Let the distribution be given in polar coordinates r and ϕ (Fig. B2).

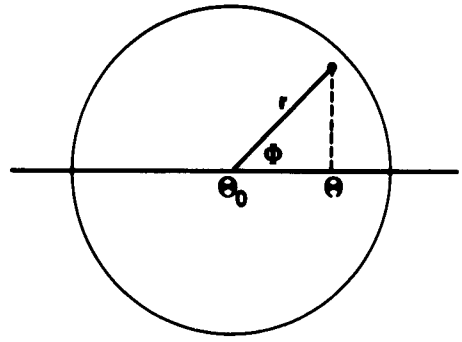

SPECIFICATION OF INTENSITY DISTRIBUTION IN POLAR COORDINATES

FIG. B2

Changing the notation of Eq. B2, and integrating over area, gives

$$S(t) = \iint P(r,\phi,t) \cos(\omega_a t+\phi_a+\frac{2\pi d}{\lambda} \sin\theta_o - \frac{2\pi d}{\lambda}\theta_o \cos\theta_o+\theta\frac{2\pi d}{\lambda}\cos\theta_o)r\, dr\, d\phi$$

From Figure B2.

$$\theta = r\cos\phi + \theta_o$$

yielding

$$(B5)\quad S(t) = \int_0^{2\pi}\int_0^R P(r,\phi,t) \cos(\omega_a t+\phi_a+\frac{2\pi d}{\lambda} \sin\theta_o +\frac{2\pi d}{\lambda}\cos\theta_o r\cos\phi)\, r\, dr\, d\phi$$

Radial symmetry

In the event the distribution depends only on r, the integration with respect to ϕ can be carried out immediately.

$$S(t) = \cos(\omega_a t+\phi_a+\frac{2\pi d}{\lambda}\sin\theta_o)\iint P(r,t)\cos\left[\frac{2\pi d}{\lambda}(\cos\theta_o)\, r\cos\phi\right]r\, dr\, d\phi$$

$$- \sin(\omega_a t+\phi_a+\frac{2\pi d}{\lambda}\sin\theta_o)\iint P(r,t)\sin\left[\frac{2\pi d}{\lambda}(\cos\theta_o)\, r\cos\phi\right]r\, dr\, d\phi$$

Integration with respect to ϕ shows the second term is zero. Therefore

$$S(t) = \cos(\omega_a t+\phi_a+\frac{2\pi d}{\lambda}\sin\theta_o)\iint P(r,t)\cos\left[\frac{2\pi d}{\lambda}(\cos\theta_o)r\cos\phi\right]r\,dr\,d\phi$$

But $\quad 2\pi J_o(x) = \int_0^{2\pi}\cos(x\cos\phi)\,d\phi$

Therefore

$$\text{(B6)}\quad S(t) = 2\pi\cos(\omega_a t+\phi_a+\frac{2\pi d}{\lambda}\sin\theta_o)\int_0^R P(r,t)\,J_o\left[\frac{2\pi d}{\lambda}(\cos\theta_o)r\right]r\,dr$$

Inverse Fourier transform relations

Knowing how the received signal varies with the baseline length, it is possible to infer some information on the source distribution. The received signal, for a distribution symmetrical about θ_o, is

$$\text{(B4)}\quad S(t) = \cos(\omega_a t + \phi_a + \frac{2\pi d}{\lambda}\sin\theta_o)\int P(\theta',t)\cos\left[\frac{2\pi d}{\lambda}(\cos\theta_o)\theta'\right]d\theta'$$

Define $A = \frac{2\pi d}{\lambda}\cos\theta_o$. Writing explicitly the dependence of S on A,

$$S(A,t) = \cos(\omega_a t + \phi_a + \frac{2\pi d}{\lambda}\sin\theta_o)\int P(\theta,t)\cos A\theta'\,d\theta'$$

If, over the observation time, the source distribution does not change, then the amplitude of the sine wave at frequency ω_a can be written

$$\text{(B7)}\quad \overline{S(A)} = \int_{-\Delta\theta'}^{\Delta\theta'} P(\theta')\cos A\theta'\,d\theta'$$

$$= 2\int_0^{\Delta\theta'} P(\theta')\cos A\theta'\,d\theta' \text{ (symmetrical case)}$$

The inverse transform can be taken

$$\text{(B8)}\quad P(\theta') = \frac{1}{\pi}\int_0^{\infty}\overline{S(A)}\cos A\,\theta'\,dA$$

which is a transform directly from baseline information to source distribution.

Similarly, in the case where the distribution is not assumed to by symmetrical, the inverse relation can be found. In this case the received signal is of the form

$$S(t) = \cos \alpha \int P(\theta) \cos A\theta \, d\theta - \sin \alpha \int P(\theta) \sin A\theta \, d\theta$$

The inverse relation is less convenient to perform, as the received signal must be separated into two components depending on difficult-to-measure phase factors in α. Once this has been done, however, the inverse transformation can be taken.

With respect to the Fourier Bessel transform, the forward relationship, in the radially symmetric case, was found to be

$$(B6) \quad S(A,t) = 2\pi \cos (\omega_a t + \frac{2\pi d}{\lambda} \sin \theta_o + \phi_a) \int_0^R P(r,t) \, J_o(Ar) \, r \, dr$$

The amplitude, for the time invariant case, is

$$\overline{S(A)} = 2\pi \int_0^R P(r) \, J_o (Ar) \, r \, dr$$

Taking the inverse transform yields

$$(B9) \quad P(r) = \frac{1}{2\pi} \int_0^\infty \overline{S(A)} \, J_o (Ar) \, A \, dA$$

<u>The inverse relation in the experimental case</u>

While a relation such as (B9) can be written to give the source distribution in terms of the received power as a function of baseline length, it is inconvenient to obtain the complete function of received power vs. baseline length. Thus approximations and assumptions must be resorted to.

One approach is to make an assumption as to the nature of the source distribution, leaving a number (n) of undetermined parameters. Then, by utilising n baselines, it is possible to get n equations in n unknowns, and solve for the source distribution, subject to the initial assumption. Two examples of this technique will be given.

Rectangular distribution

Assume that $P(\theta')$ is constant in an interval:

$$P(\theta') = \text{constant}, \quad -\Delta\theta' \leq \theta' \leq +\Delta\theta'$$

$$= 0 \qquad \text{otherwise}$$

Then

$$\overline{S(A)} = P \int_{-\Delta\theta'}^{\Delta\theta'} \cos A\theta' \, d\theta' \tag{B7}$$

$$= 2P\Delta\theta' \frac{\sin A\Delta\theta'}{A\Delta\theta'} \tag{B10}$$

There are two unknowns, P and $\Delta\theta'$. Therefore, the use of two baselines, corresponding to A_1 and A_2 will yield a solution:

$$\overline{S(A_1)} = 2P\Delta\theta' \frac{\sin A_1 \Delta\theta'}{A_1 \Delta\theta'}$$

$$\overline{S(A_2)} = 2P\Delta\theta' \frac{\sin A_2\Delta\theta'}{A_2 \Delta\theta'}$$

Minimum baseline

For the solution of these two equations, it is necessary that the two values of $\overline{S(A)}$ be different. If A_1 is small, then A_2 must be large enough to give a result measurably different from A_1. Assume that d_1 is sufficiently small so that $\frac{\sin A_1\Delta\theta'}{A_1\Delta\theta'} \cong 1$, and arbitrarily define the limit of source resolution such that $\frac{\overline{S(A_2)}}{\overline{S(A_1)}} \leq 0.9$.

Then

$$\frac{\sin A_2 \Delta\theta}{A_2 \Delta\theta} = 0.9, \text{ from which } A_2\Delta\theta = \pi/4$$

The requirement on d_2 is therefore

$$(B11) \qquad d_2 \geq \frac{\lambda}{8 (\cos \theta_o)\Delta\theta}$$

For $\lambda = 1.524$ meters, $\theta_o = 0$, and converting to degrees, this is equivalent to

$$(B12) \qquad d_2 \geq \frac{72'}{\Delta D}$$

where ΔD is the source diameter (instead of radius) in degrees.

Uniform radial distribution

In this case

$$(B6) \qquad \overline{S(A)} = \frac{2\pi P}{A^2} \int_0^R J_o(Ar)\ (Ar)\ d\ (Ar)$$

$$(B13) \qquad = \pi R^2 P \frac{2\ J_1\ (Ar)}{Ar}$$

For $\frac{2\ J_1\ (x)}{x} = .9$,

$$x \cong .91$$

Using the same criterion for minimum baseline that was used in the rectangular case, we get, corresponding to (B11) and (B12) respectively,

$$(B14) \qquad d_2 \geq \frac{.91\ \lambda}{2\pi\ R \cos \theta_o}$$

and

$$(B15) \qquad d_2 \geq \frac{83'}{D}$$

where in (B15) $\theta_o = 0$, $\lambda = 1.524$, and $D = 2R$, converted to degrees.

Reduction in power for simultaneous position and frequency distribution

The received signal in the symmetrical case was found to be

$$(B4)\quad S(t) = \cos(\omega_a t+\phi_a+\frac{2\pi d}{\lambda}\sin\theta_o)\int_{-\Delta\theta}^{+\Delta\theta} P(\theta',t)\cos\left[\frac{2\pi d}{\lambda}(\cos\theta_o)\theta'\right]d\theta'$$

The power distribution can be represented as a distribution in frequency as well as in space. Since superposition holds, the received signal is of the form

$$(B16)\quad S(t)=\iint\cos(\omega_a t+\phi_a+\frac{2\pi df}{c}\sin\theta_o)\cos\left[\frac{2\pi df}{c}(\cos\theta_o)\theta'\right]P(\theta',f)d\theta'df'$$

A straightforward integration immediately involves integrals of the form $\frac{\sin x}{x}\,dx$. These are inconvenient to work with. However, for large x, and for a small range of integration, the approximation

$$(B17)\qquad \int\frac{\sin x}{x}\,dx \simeq \frac{1}{x}\int\sin x\,dx$$

can be used.

Assume that $P(\theta',f)$ is constant over its range of θ' and f. Integrating (16) with respect to θ' gives

$$S(t) = \frac{Pc}{\pi df'\cos\theta_o}\int_{f_1}^{f_2}\cos(\omega_a t+\frac{2\pi df}{c}\sin\theta_o+\phi_a)\sin(\frac{2\pi df}{c}\Delta\theta\cos\theta_o)df$$

where $f' = \frac{f_1+f_2}{2}$ and $\frac{1}{f}$, has been taken out as in (17).

Performing a trigonometric expansion yields

$$S(t)=\frac{Pc}{2\pi df'\cos\theta_o}\int_{f_1}^{f_2}\sin\left[\omega_a t+\phi_a+\frac{2\pi df}{c}(\sin\theta_o+\Delta\theta\cos\theta_o)\right]df$$

$$-\frac{Pc}{2\pi df'\cos\theta_o}\int_{f_1}^{f_2}\sin\left[\omega_a t+\phi_a+\frac{2\pi df}{c}(\sin\theta_o-\Delta\theta\cos\theta_o)\right]df$$

Integration and further expansion yields

$$S(t)=\frac{2P}{f'\cos\theta_o}\left(\frac{c}{2\pi d}\right)^2\left\{\frac{\sin\left[\frac{\pi d}{c}\Delta f(\sin\theta_o+\Delta\theta\cos\theta_o)\right]\cos\left[\frac{2\pi d}{c}f'(\sin\theta_o+\Delta\theta\cos\theta_o)\right]}{\sin\theta_o+\Delta\theta\cos\theta_o}\right.$$

$$- \frac{\sin\left[\frac{\pi d}{c}\,\Delta f(\sin\theta_o - \Delta\theta\cos\theta_o)\right]\cos\left[\frac{2\pi d}{c}f'(\sin\theta_o - \Delta\theta\cos\theta_o)\right]}{\sin\theta_o - \Delta\theta\cos\theta_o}\Bigg\}\sin(\omega_a t+\phi_a)$$

$$+\frac{2P}{f'\cos\theta_o}\left(\frac{c}{2\pi d}\right)^2\Bigg\{\frac{\sin\left[\frac{\pi d}{c}\Delta f(\sin\theta_o+\Delta\theta\cos\theta_o)\right]\sin\left[\frac{2\pi d}{c}f'(\sin\theta_o+\Delta\theta\cos\theta_o)\right]}{\sin\theta_o + \Delta\theta\cos\theta_o}$$

$$-\frac{\sin\left[\frac{\pi d}{c}\Delta f(\sin\theta_o-\Delta\theta\cos\theta_o)\right]\sin\left[\frac{2\pi d}{c}f'(\sin\theta_o-\Delta\theta\cos\theta_o)\right]}{\sin\theta_o - \Delta\theta\cos\theta_o}\Bigg\}\cos(\omega_a t + \phi_a)$$

where $\Delta f = f_2 - f_1$, and $f' = \frac{f_1 + f_2}{2}$

Let

$$\text{(B18)}\quad A=2P\Delta f\Delta\theta\,\frac{1}{\Delta\theta\cos\theta_o}\left(\frac{f'}{\Delta f}\right)\left(\frac{\lambda'}{2\pi d}\right)^2\frac{\sin\frac{1}{2}\left(\frac{2\pi d}{\lambda'}\right)\left(\frac{\Delta f}{f'}\right)(\sin\theta_o+\Delta\theta\cos\theta_o)}{\sin\theta_o + \Delta\theta\cos\theta_o}$$

$$\text{(B19)}\quad B=2P\Delta f\Delta\theta\,\frac{1}{\Delta\theta\cos\theta_o}\left(\frac{f'}{\Delta f}\right)\left(\frac{\lambda'}{2\pi d}\right)^2\frac{\sin\frac{1}{2}\left(\frac{2\pi d}{\lambda'}\right)\left(\frac{\Delta f}{f'}\right)(\sin\theta_o-\Delta\theta\cos\theta_o)}{\sin\theta_o - \Delta\theta\cos\theta_o}$$

$$a = \frac{2\pi d}{\lambda'}(\sin\theta_o + \Delta\theta\cos\theta_o)$$

$$b = \frac{2\pi d}{\lambda'}(\sin\theta_o - \Delta\theta\cos\theta_o)$$

$$\text{(B20)}\quad a-b = 2\left(\frac{2\pi d}{\lambda'}\right)\Delta\theta\cos\theta_o$$

Then

$$S(t) = (A\cos a - B\cos b)\sin(\omega_a t + \phi_a)$$

$$+ (A\sin a - B\sin b)\cos(\omega_a t + \phi_a)$$

Taking the square of both components of $(\omega_a t + \phi_a)$ will give the amplitude squared of $S(t)$:

$$\text{(B21)}\quad \bar{S}^2 = A^2 + B^2 - 2AB\cos(a - b)$$

Thus, the amplitude of the received signal can be found by solving the following triangle

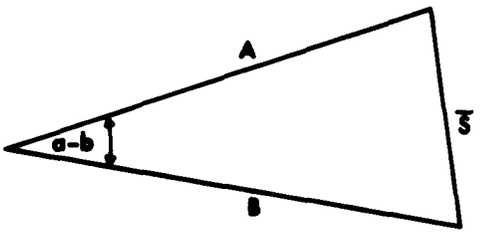

Special case, frequency distribution only

In the case of a point source with finite bandwidth, the solution reduces to

$$(B22) \qquad \bar{S} = 2P\Delta f\Delta\theta \frac{\sin(\frac{\pi d}{c}\Delta f \sin\theta_o)}{\frac{\pi d}{c}\Delta f \sin\theta_o}$$

$$= 2P\Delta f\Delta\theta \frac{\sin\left[\frac{1}{2}\left(\frac{2\pi d}{\lambda}\right)\left(\frac{\Delta f}{f}\right)\sin\theta_o\right]}{\frac{1}{2}\left(\frac{2\pi d}{\lambda}\right)\left(\frac{\Delta f}{f}\right)\sin\theta_o}$$

Example

The received amplitude for the following case, with both frequency and source spread, will be evaluated:

$\frac{2\pi d}{\lambda} = 380$

$\frac{\Delta f}{f} = 0.01154$

$\Delta\theta = .01$ radian

$\theta_o = 60°$

If $\Delta\theta$ were zero, the received signal would be by (22)

$$\bar{S} = 2\,P\Delta f\Delta\theta \frac{\sin 1.9}{1.9}$$

$$= (2\,P\Delta f\Delta\theta) \times \frac{1}{2}$$

which is a 50% reduction in power.

If $\frac{\Delta f}{f}$ were zero, then by (10)

$$\overline{S} = 2\,P\Delta f\Delta\theta\,\frac{\sin 1.9}{1.9} = (2\,P\Delta f\Delta\theta) \times \frac{1}{2},$$

also equal to $\frac{1}{2}$. For the combined case,

$$A = 2\,P\Delta f\Delta\theta \times .13$$

$$B = 2\,P\Delta f\Delta\theta \times .1323$$

$$a-b = 3.8 \text{ radians} = 218° = -142°$$

Therefore, solving the triangle gives

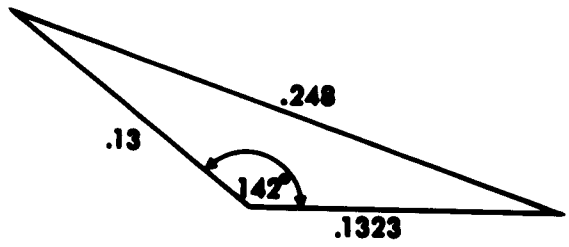

The received signal is then

$$(2P\Delta f\Delta\theta) \times .248$$

REFERENCES

1. Little, A. G., Payne-Scott, Ruby
   Aust. J. Phys. A4, 489 (1951)

2. Ryle, M.
   Proc. Roy. Soc. A211, 351 (1952)

3. Penfield, H.
   Proc. IRE, 46, 321 (1958)

4. Hanbury Brown, R., Palmer, H. P., Thompson, A. R.
   Phil. Mag. 7, 46 (1955)

5. Cohen, M. H.
   Proc. IRE, 46, 183 (1958)

6. Simas, V. R., Bartholomew, C. A.
   Project Vanguard Report No. 23
   NRL Report 5055 (1957)

7. Berbert, J. H.
   IRE Trans. Inst. I-9, 84 (1960)

8. Fleischer, R., Oshima, M.
   Paper given at the 107th Meeting of The American
   Astron ical Society (Dec. 30, 1960)

9. Wild, J. P., Sheridan, K. V.
   Proc. IRE. 46, 160 (1958)

10. Boischot, A.
    Annales d'Astrophysique 21, 273 (1958)

11. Firor, J., Paper 24 given at Paris Symposium on Radio
    Astronomy
    Stanford U., Stanford, (1959)
    (R. N. Bracewell, Ed.)

12. Owren, L.
    Radio Astronomy Report No. 15 (May 1954), Cornell University

13. Fokker, A. D.
    Ph.D. Thesis, "Studies of Enhanced Solar Radio Emission
    at Frequencies Near 200 MC"
    State University of Leiden, June 22, 1960

14. Terman, F. E., Radio Engineers Handbook
    McGraw-Hill, New York, 210, (1943)

15. Ryle, M., and Vonberg, D. D.
Proc. Roy. Soc. 193, 98 (1948)

16. Landee, Davis and Albrecht
Electronic Designer's Handbook
McGraw-Hill, New York, 16-20 (1957)

17. Millman, J. and Taub, H.
Pulse and Digital Circuits
McGraw-Hill, New York, 117 (1956)

18. Whitfield, G. R., Paper 58
Paris Symposium on Radio Astronomy
Stanford U., Stanford (1959)
(R. N. Bracewell, Ed.)

19. McReady, L. L., Pawsey, J. L., and Payne-Scott, Ruby
Proc. Roy. Soc., A190, 357 (1947)

20. Pawsey, J. L. and Bracewell, R. N.
Radio Astronomy
Clarendon, Oxford, 57 (1955)

21. Payne-Scott, Ruby, and McReady, L. L.
Terr. Mag. 53, 429 (1948)

22. Bailey, D. K.
Terr. Mag. 53, 41 (1948)

23. Little, C. G., Rayton, W. M., and Roof, R. B.
Tech. Report No. 1, Contract No. A.F. 30 (635)-2887

24. Smith, F. G.
J.A.T.P. 2, 350 (1952)

25. Hewish, A.
Proc. Roy. Soc. 214, 494 (1952)

26. Lawrence, R. S., Jespersen, J. L. and Lamb, R. C.
J. of Res. NBS 65, No. 4, (1961)

27. Booker, H. G.
Proc. IRE, 46, 298 (1958)

28. Kretzmer, E. R.
Electronics, 22, 114 (1949)

29. Schwartz, S.
Selected Semiconductor Circuits Handbook
John Wiley, New York, 6-36 (1960)